

PENETRATION OF NANOPARTICLES INTO A BIOFILM FROM A BULK
FLUID

A Thesis

Presented to

The Graduate Faculty of The University of Akron

In Partial Fulfillment

of the Requirements for the Degree

Master of Science

Ryan Neubig

December, 2011

PENETRATION OF NANOPARTICLES INTO A BIOFILM FROM A BULK
FLUID

Ryan Neubig

Thesis

Approved:

Advisor
Gerald Young

Accepted:

Dean of the College
Chand Midha

Co-Advisor
Kevin Kreider

Dean of the Graduate School
George Newkome

Co-Advisor
Curtis Clemons

Date

Co-Advisor
Patrick Wilber

Department Chair
Timothy Norfolk

ABSTRACT

A biofilm is a sessile community of microorganisms embedded in a self-secreted matrix composed of extracellular polymeric substance. Biofilms display an increased resistance to antimicrobial agents and host clearance mechanisms. We develop a mathematical model to simulate the transport and deposition of nanoparticles in the deep passages of the lungs infected with biofilm. The nanoparticles are vessels for antimicrobial agents, and upon penetration into the biofilm via diffusion, the particles degrade and release the antimicrobial into the surrounding ecology. In our model a solution of polymer-PLGA nanoparticles is injected into a parallel-plate flow cell. The flow cell has a substrate of biofilm of known surface morphology. Then, a mucus barrier, similar to those found in the lungs of patients with cystic fibrosis, is introduced to the surface of the biofilm to investigate its effects on nanoparticle diffusion into the biofilm. The system of governing equations describing the model is reduced to two coupled partial differential equations though asymptotic expansion, and is solved using numerical methods. We compare the effects of system variables and mucus on nanoparticle concentrations in the biofilm. We find the sensitivity of our model to changes in the magnitude of system variables, and how the addition of a mucus barrier over the biofilm affects nanoparticle penetration into the biofilm.

ACKNOWLEDGEMENTS

I am deeply indebted to my advisors Dr. Gerald Young, Dr. Kevin Kreider, Dr. Curtis Clemons and Dr. Patrick Wilber who graciously gave their time and patience to see this thesis to fruition.

I would like to give my special thanks to my wife, Ashley, whose patient love enable me to complete this work.

TABLE OF CONTENTS

	Page
LIST OF TABLES	vii
LIST OF FIGURES	viii
CHAPTER	
I. INTRODUCTION	1
1.1 Background on Biofilms and Cystic Fibrosis	1
1.2 Previous Modeling of Biofilms and Mucosa	2
1.3 Abbreviated Description of Our Model	5
1.4 Summary of Our Results and Thesis Outline	7
II. FORMULATION OF THE MODEL	9
2.1 The Governing Equations	9
2.2 Boundary and Initial Conditions	11
2.3 Nondimensional Forms of the Simplified Governing Equations and Conditions	14
III. SOLUTION PROCEDURE	19
3.1 Asymptotic Techniques	19
3.2 Numerical Solution of the System of Equations	23

IV. RESULTS	29
4.1 Effects of System Variables on Nanoparticle Concentration	29
4.2 Effects of a Mucus Barrier on Nanoparticle Absorption	43
V. SUMMARY	50
BIBLIOGRAPHY	52
APPENDIX	55

LIST OF TABLES

Table	Page
2.1 System variables, characteristic scalings and their units	15
3.1 Values for system variables used in the solution procedure	28
4.1 System parameters used for 4.1.1	30
4.2 System parameters used for subsection 4.1.2	33
4.3 System parameters used for subsection 4.1.3	38
4.4 System parameters used for 4.2.1	44

LIST OF FIGURES

Figure	Page
1.1 The geometry of the flow cell modeled in the simulations. The fluid is characterized by a steady-state, laminar, pressure-driven flow that is parabolic in nature. The height of the biofilm \tilde{h} is a known function of horizontal position \tilde{x} . The length of the flow cell $L = 4.0$ cm and the height d between plates is 0.1 cm.	5
2.1 The nondimensionalized schematic of the parallel-plate flow cell. In addition to the biofilm on the substrate, a mucus layer approximately 10% the height of the biofilm is added atop the biofilm.	16
4.1 This simulation compares the changes mass diffusivity of the biofilm D_B has on the concentration profiles in the biofilm. $D_B = 1.0 \times 10^{-7}$, 1.0×10^{-8} and $1.0 \times 10^{-9} \frac{\text{cm}^2}{\text{s}}$, and the three lines represent concentration values as a function of biofilm depth at the horizontal position $x = 1$ cm and at the time $t = 72$ min in the flow cell.	31
4.2 The concentration plug flowing through the flow cell is depicted. We show four concentration profiles occurring at times between 43.2 min and 86.4 min. The dilute concentration of the plug and the relatively low sticking coefficient K prevent the profile from changing radically. Also, the profile of the biofilm surface does not influence the spacing between peaks.	32
4.3 The time evolution of concentration of nanoparticles in the biofilm C_B with flow rate $Q = 1.0 \times 10^{-5} \frac{\text{cm}^3}{\text{s}}$. The biofilm concentration function C_B is measured at $x = 1.0$ cm, and we show the concentration profile from time $t = 28.6$ min to $t = 86.4$ min.	34

4.4	The time evolution of nanoparticle concentrations in the biofilm. The flow rate is decreased to $1.0 \times 10^{-6} \frac{\text{cm}^3}{\text{s}}$, and we see the concentration of nanoparticles begins to rise at time $t = 302.4$ min. The time evolution of concentration is like that of Figure 4.3, but due to the smaller flow rate Q , the flux of particles occurs over a greater time period. The concentration profile at $t = 331.2$ min has a more dramatic rise as a result of the decreased flow rate.	35
4.5	This figure shows the narrow concentration profile resulting from decreasing the flow rate Q from 1.0×10^{-5} to $1.0 \times 10^{-6} \frac{\text{cm}^3}{\text{s}}$	37
4.6	The concentration profile for the case $Q = 1.0 \times 10^{-5} \frac{\text{cm}^3}{\text{s}}$, $D_B = 1.0 \times 10^{-7} \frac{\text{cm}^2}{\text{s}}$ and $S_c = 1.0 \times 10^{-7} \frac{\text{cm}}{\text{s}}$	39
4.7	The concentration profile of the nanoparticle plug passing through the flow cell with an increase in the sticking coefficient S_c . By changing the sticking coefficient from 1.0×10^{-7} to $1.0 \times 10^{-6} \frac{\text{cm}}{\text{s}}$, we can begin to see absorption of nanoparticles into the biofilm as time progresses from $t = 57.6$ to $t = 86.4$ min.	40
4.8	The concentration profile for the case $Q = 1.0 \times 10^{-5} \frac{\text{cm}^3}{\text{s}}$, $D_B = 1.0 \times 10^{-7} \frac{\text{cm}^2}{\text{s}}$ and $S_c = 1.0 \times 10^{-5} \frac{\text{cm}}{\text{s}}$	41
4.9	Surface plots for three values of the sticking coefficient (a) $S_c = 1.0 \times 10^{-7}$, (b) 1.0×10^{-6} , (c) $1.0 \times 10^{-5} \frac{\text{cm}}{\text{s}}$	42
4.10	The introduction of mucus to the top 10% of the biofilm structure is depicted in this figure. The mass diffusivity of mucus $D_M = 1.0 \times 10^{-8} \frac{\text{cm}^2}{\text{s}}$ rapidly decreases concentration profiles with magnitudes much less than those found in a pure biofilm substrate. We see a region of exponential decrease at an increased rate in the top tenth of the biofilm followed by a much gentler decrease in concentration of nanoparticles at depths in the biofilm.	45
4.11	This figure depicts the effects of a decreased mucus mass diffusivity constant $D_M = 1.0 \times 10^{-9} \frac{\text{cm}^2}{\text{s}}$ on the nanoparticles' ability to penetrate through the additional mucus barrier. We see a rapid decrease in the concentration profile in the top 10% of the biofilm followed by a shallow exponential decay of concentration into the remaining depth of the biofilm structure.	46
4.12	The concentratino profile for the case $Q = 1.0 \times 10^{-5} \frac{\text{cm}^3}{\text{s}}$, $D_B = 1.0 \times 10^{-7} \frac{\text{cm}^2}{\text{s}}$, $D_M = 1.0 \times 10^{-6} \frac{\text{cm}^2}{\text{s}}$ and $S_c = 1.0 \times 10^{-7} \frac{\text{cm}}{\text{s}}$	47

CHAPTER I

INTRODUCTION

1.1 Background on Biofilms and Cystic Fibrosis

A biofilm is a sessile community of microorganisms embedded in a self-secreted matrix composed of extracellular polymeric substance (EPS). Bacterial biofilms cause life-threatening diseases in patients with chronic respiratory infections. Typically, lung biofilms are composed of *Pseudomonas aeruginosa*, *Staphylococcus aureus* and/or *Haemophilus influenzae*, and these organisms display an increased resistance to antimicrobial agents and host clearance mechanisms [1, 2, 3, 4, 5, 6, 7]. When biofilms are able to form in the lungs of an immunocompromised host, their removal using conventional antibiotic treatments is unlikely.

Chronic respiratory infections have been recognized as having the greatest role in the morbidity and mortality of those afflicted with cystic fibrosis (CF). CF is the most common life-shortening autosomal recessive disease in the caucasian population, afflicting over 30,000 persons in the United States [8] . The patient's defective mucosilary clearance promotes mucus retention in the lungs. Mucus serves as a nutrient-rich food source and physical barrier allowing biofilms to grow unhindered and remain impenetrable to conventional antibiotics [9]. CF lung diseases are char-

acterized by an exaggerated inflammatory response, progressive airway obstruction, bronchiectasis and eventually, respiratory failure [10]. As a result, 90% of patients die prematurely [11]. A large patient population without an effective course of treatment is driving a global effort to develop a safe and effective drug delivery system to kill bacterial biofilm infections of the lung.

Administering respiratory medications via inhalation is often achieved through nebulization – the process of breaking up medical solutions into small aerosolized droplets. This delivery system allows for localized treatment of biofilms while minimizing adverse systemic reactions to antimicrobial compounds. Numerous systemic variables affect how inhaled particulates distribute in the lungs; however, more efficient deposition patterns can be achieved by understanding how physical and chemical properties of nanoparticles affect transport throughout the pulmonary region. For example, particle surface properties can cause significant aggregation of micron-sized particles, reducing the efficiency of deep lung deposition [12].

1.2 Previous Modeling of Biofilms and Mucosa

Longest and Oldham [13] develop a model for simulating the regional and local deposition in the major regions of the respiratory tract. Their research indicates the deposition efficiency of aerosols depends on lung morphology, fluid motion and characteristics of the inhaled particulate. Although the deposition efficiency tends to be low, the research does indicate that transient inhalation flow can be closely ap-

proximated by steady flow conditions, and hence, most computational fluid dynamics simulations assume steady particle flow.

Like Longest and Oldham, most of the theoretical studies of aerosol distributions in an airway model the lung passages as a bifurcating network of cylindrical pipes. The effects of this idealization on regional and local deposition patterns in different parts of the respiratory tract remain largely unquantified [14]. We draw from multiple studies to build a theoretical model of nanoparticle adhesion and diffusion at the local level.

The studies of Drury et al. [15, 16] examine two models and provide key insights into nanoparticle penetration of biofilms at the local level. They examine the concentration levels of fluorescent latex microbeads added to a biofilm in a rotating annular reactor and also develop a mathematical model assuming advective displacement as a means of particle transport within the biofilm. The advection model predicted a significant release of latex tracers back into the bulk fluid after particle injection ceased, which is not observed microscopically in biofilm tissue. Microbeads added in the bulk liquid become distributed throughout the biofilm depth of $30 \mu\text{m}$ in 24 hours suggesting the existence of a non-advective transport mechanism.

The results of Drury et al. indicate diffusion, not advection, as being the dominate mechanism for transport in a biofilm. The authors postulated that the surface roughness and pore structure provide a conduit for the beads to move into the biofilm, which has a mean pore diameter of approximately $2.0 \mu\text{m}$ in the top layers to about $0.3 \mu\text{m}$ in the bottom layers [17]. Given these diameters, nanoscale

particles should be able to penetrate the biofilm surface through this pore structure. These authors also found the mass diffusivity of microbeads in water, a value which we use in our numerical solution.

Klapper et al. [18] provide support for diffusion being the dominant form on particle transport in a biofilm. They develop a mathematical model describing the constitutive properties of biofilms so as to predict biofilm deformation under stress and strain. They conclude biofilms behave as viscoelastic fluids, so it can be assumed the diffusivity of nanoparticles in a biofilm must occur on much greater time scales than the diffusivity in the carrier fluid. The interior of a biofilm is a dynamic environment full of voids, crevasses, and pores, so assuming a biofilm is a continuous viscous structure can only yield rough estimates of particle transport within the biofilm. Although this view of biofilm structure is simple, numerical results by Klapper et al. are in good agreement with experimental findings.

The series of works by Hanes *et al.* [19, 20, 21, 22] provide a comprehensive review of nanoparticle penetration into mucus barriers. They engineer nanoparticles that are densely coated with poly(ethylene glycol), which can rapidly penetrate mucus by minimizing mucoadhesion. We will assume nanoparticles coated with PEG can slip through a mucus barrier with an effective mass diffusivity in mucus that is greater than that of uncoated nanoparticles but lesser than that of nanoparticles passing through water.

1.3 Abbreviated Description of Our Model

In this thesis, we will develop a mathematical model motivated by transport and deposition of nanoparticles in the deep passages of the lungs infected with biofilm. Our research uniquely addresses the effects of nanoparticle adhesion characteristics on particle penetration into the biofilm and how mass diffusivity affects diffusion throughout the biofilm. Also, we introduce a mucus covering to the biofilm surface to measure the effect on nanoparticle concentration at multiple depths of the biofilm structure.

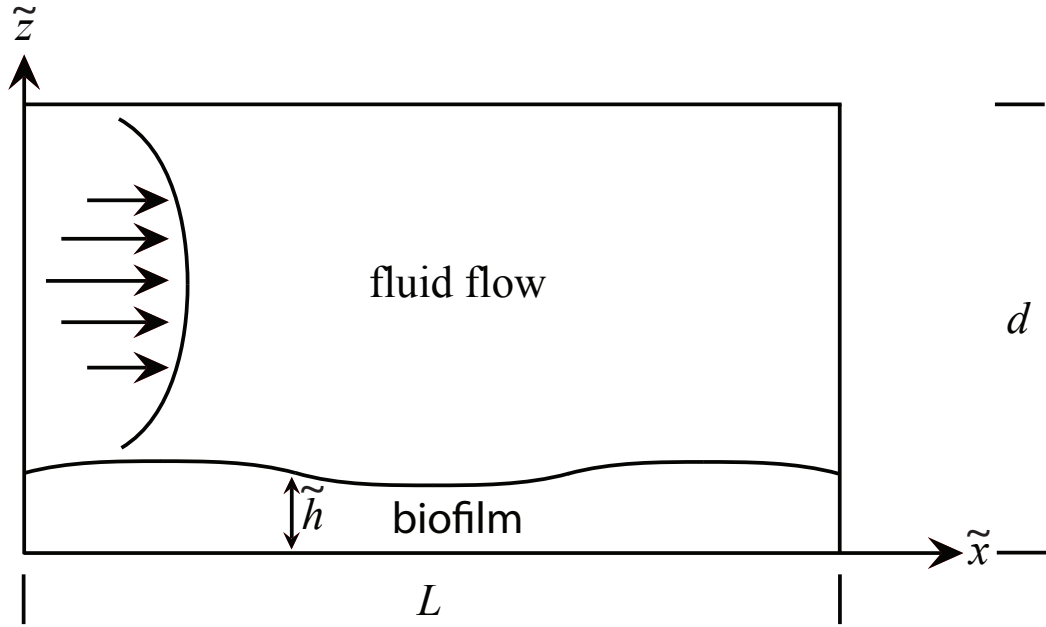


Figure 1.1: The geometry of the flow cell modeled in the simulations. The fluid is characterized by a steady-state, laminar, pressure-driven flow that is parabolic in nature. The height of the biofilm \tilde{h} is a known function of horizontal position \tilde{x} . The length of the flow cell $L = 4.0$ cm and the height d between plates is 0.1 cm.

We now discuss reasoning for choosing the appropriate equations to model

nanoparticle transport. Fluid flow in the airway can be closely characterized by the non-linear Navier-Stokes equations. Due to the long thin geometry of the deep passages of the lungs, the time dependent chaotic behavior of the fluid can be ignored. We assume a steady, parallel, non-convective pressure-driven flow in the region of interest, and therefore, we assume particle transport in the lungs resembles fluid flow between two parallel plates. The resulting boundary value problem can be solved using no slip conditions at the fluid-biofilm and fluid-tissue interfaces.

Our model assumes adhesion as the primary mechanism for nanoparticle capture by the biofilm. Engineered with particular adhesion characteristics, biodegradable polymer adheres to tissue structure in the respiratory tract. The size of the nanoparticles allows individual particles to penetrate deeply into the biofilm's cavity and pore structure. The work by Luna et al. [23] models biofilm development including formation of cavities and pores within the structure. Their results show particle profiles depend mainly on biofilm thickness and to a lesser degree on heterogeneities in porosity and permeability. Once the nanoparticles are captured by the biofilm or by a mucus layer, diffusion, presumed to be the primary form of nanoparticle transport, distributes the nanoparticles through the EPS matrix.

We examine the particle concentration in the biofilm up to twenty-four hours after the injection of the nanoparticles. During this time, changes in biofilm depth and surface morphology are insignificant. The boundary between the biofilm and carrier fluid is assumed to be constant in time, depending only upon the horizontal position with respect to the substrate. We assume the biofilm surface has a sinusoidal

profile and an average depth much thinner than the biofilm length.

1.4 Summary of Our Results and Thesis Outline

We develop a model in which asymptotic expansion is used to produce a coupled system of equations. We use a diffusion-advection equation, Navier-Stokes equations, and mixed boundary conditions to produce a leading order one-dimensional time evolution equation for concentration as the nanoparticle plug passes through the flow cell. For the biofilm region, a pure diffusion equation with Neumann boundary conditions is used to produce a leading-order time evolution equation for nanoparticle concentration in the biofilm. We use the Lax-Wendroff and Crank-Nicolson methods to solve the advection and diffusion equations, respectively, numerically. Despite being leading order, our results should give good approximations to experimental observations, which is the next step in verifying the model.

The values of the mass diffusivity in biofilm, the sticking characteristics of polymer PLGA nanoparticles, and the average flow rates in the deep passages of the pulmonary system are unknown. We will vary the magnitude of these system parameters over several orders of magnitude to illustrate the sensitivity of the results to errors in parameter measurement.

In this thesis we show the flow rate Q alters the profile of the concentration plug traveling through the flow cell, but large changes in nanoparticle concentrations in the biofilm are not observed as a result of a decreased flow rate. The sticking coefficient parameter S_c limits the flux of nanoparticles passing through the fluid/biofilm

interface. As the sticking coefficient is increased in our model, we observe a large increase in nanoparticle concentrations in the biofilm. A thin mucus barrier can greatly diminish the ability of the nanoparticles from penetrating the biofilm. If the surface mucoadhesivity of the nanoparticles can be decreased with a surface coating, as proposed by Hanes et al., the nanoparticles in our model slip through the mucus barrier and penetrate uniformly into the biofilm.

For clarity, we now list the assumptions used in the formulation of our model.

1. The carrier fluid contains a well mixed dilute concentration of nanoparticles
2. Fluid flow is parabolic, laminar, and steady state
3. No flux and no slip boundary conditions are imposed at geometry boundaries
4. Nanoparticle adhesion is the main mode of capture at a biofilm surface
5. Diffusion is the dominant form of particle transport in the biofilm
6. System variables can be approximated by asymptotic series

We continue by formulating the mathematical model in Chapter II, where we introduce characteristic scalings to nondimensionalize the governing equations and boundary conditions. Chapter III describes the solution to the problem. Asymptotic expansion yields a coupled system of leading order partial differential equations, which we solve using numerical techniques. The results are presented in Chapter IV, and interpretations of the data are given. The thesis concludes in Chapter V with a summary of the important findings resulting from our investigation.

CHAPTER II

FORMULATION OF THE MODEL

In this chapter, the governing equations used to describe the mathematical models of nanoparticles transport in the liquid and biofilm. We will discuss the characteristic scalings used to non-dimensionalize the governing equations.

2.1 The Governing Equations

Nanoparticle transport in the carrier fluid is modeled by the equations that follow defined in the fluid domain shown in Figure 1.1.

The Navier-Stokes equations, which govern the velocity field of the carrier fluid, are given by

$$\rho[\tilde{u}_{\tilde{t}} + \tilde{u}\tilde{u}_{\tilde{x}} + \tilde{w}\tilde{u}_{\tilde{z}}] = -\tilde{P}_{\tilde{x}} + \mu[\tilde{u}_{\tilde{x}\tilde{x}} + \tilde{u}_{\tilde{z}\tilde{z}}] \quad (2.1)$$

for the horizontal direction and

$$\rho[\tilde{w}_{\tilde{t}} + \tilde{u}\tilde{w}_{\tilde{x}} + \tilde{w}\tilde{w}_{\tilde{z}}] = -\tilde{P}_{\tilde{z}} + \mu[\tilde{w}_{\tilde{x}\tilde{x}} + \tilde{w}_{\tilde{z}\tilde{z}}] \quad (2.2)$$

for the vertical direction. The carrier fluid is assumed to be a dilute solution of nanoparticles, so the density ρ and viscosity μ are constants that are assumed to be

those of water. The horizontal and vertical velocities of the fluid flow are denoted by \tilde{u} and \tilde{w} , respectively, and \tilde{P} is the prescribed fluid pressure. However, like Longest and Oldham [13], we assume a steady state solution where the velocity fields are not time dependent

$$\tilde{u}_{\tilde{t}} = \tilde{w}_{\tilde{t}} = 0, \quad (2.3)$$

so equations (2.1) and (2.2) become, respectively,

$$\rho[\tilde{u}\tilde{u}_{\tilde{x}} + \tilde{w}\tilde{u}_{\tilde{z}}] = -\tilde{P}_{\tilde{x}} + \mu[\tilde{u}_{\tilde{x}\tilde{x}} + \tilde{u}_{\tilde{z}\tilde{z}}] \quad (2.4)$$

and

$$\rho[\tilde{u}\tilde{w}_{\tilde{x}} + \tilde{w}\tilde{w}_{\tilde{z}}] = -\tilde{P}_{\tilde{z}} + \mu[\tilde{w}_{\tilde{x}\tilde{x}} + \tilde{w}_{\tilde{z}\tilde{z}}]. \quad (2.5)$$

Fluid transport of nanoparticles is assumed to occur through the combination of advection and diffusion and is described by the following partial differential equation of concentration

$$\tilde{C}_{\tilde{t}} + \tilde{u}\tilde{C}_{\tilde{x}} + \tilde{w}\tilde{C}_{\tilde{z}} = D[\tilde{C}_{\tilde{x}\tilde{x}} + \tilde{C}_{\tilde{z}\tilde{z}}]. \quad (2.6)$$

The constant D is the mass diffusivity of nanoparticles in the fluid, and \tilde{C} is the time dependent concentration of the nanoparticles in the carrier fluid. Mass is conserved in the fluid region, so we use the continuity equation

$$\tilde{u}_{\tilde{x}} + \tilde{w}_{\tilde{z}} = 0. \quad (2.7)$$

Nanoparticle transport in the biofilm is modeled by the following equations defined in the biofilm domain shown in Figure 1.1. The nanoparticle diffusion equation is given by

$$\tilde{C}_{B,\tilde{t}} = D_B[\tilde{C}_{B,\tilde{x}\tilde{x}} + \tilde{C}_{B,\tilde{z}\tilde{z}}], \quad (2.8)$$

where D_B is the mass diffusivity of the nanoparticles in biofilm. The diffusivity of particles in the biofilm is much less than that of the fluid:

$$D_B \ll D. \quad (2.9)$$

Further, the advective velocities of the biofilm are assumed to be negligible, so transport of nanoparticles within the biofilm is dominated by diffusion only.

2.2 Boundary and Initial Conditions

Now, we present the boundary and initial conditions for the governing equations. At time $\tilde{t} = 0$, a well mixed solution of nanoparticles is injected into the system continuously for a period of fifteen minutes, denoted by t_{inj} . Following this time period injection ceases and the nanoparticle plug is allowed to flow through the flow cell. We describe the inlet boundary condition at $\tilde{x} = 0$ with

$$\tilde{C}(0, \tilde{z}, \tilde{t}) = A - AH(\tilde{t} - t_{inj}), \quad (2.10)$$

where A is the nanoparticle concentration of the fluid and $H(\tilde{t} - t_{inj})$ is the Heaviside function.

The height of the biofilm \tilde{h} is assumed to be a function of the horizontal direction and not of time. The time scale for a significant change in biofilm morphology is on the order of days, therefore, assuming a fixed biofilm height is apt for our purposes. The flux of nanoparticles through the interface at $\tilde{z} = \tilde{h}(x)$ is

$$D\nabla\tilde{C}\cdot\hat{n} = S_c\tilde{C}, \quad (2.11)$$

where $\nabla = \frac{\partial}{\partial\tilde{x}}\hat{i} + \frac{\partial}{\partial\tilde{z}}\hat{k}$, for unit normal vectors \hat{i} , \hat{k} in the horizontal and vertical directions, respectively, and S_c is the sticking coefficient of the nanoparticles. A non-zero sticking coefficient implies nanoparticles will stick to the surface of the biofilm if they come in contact; whereas, a value of 0 implies no particles will stick. Expanding equation (2.11) yields

$$\frac{D[-\tilde{C}_{\tilde{x}}\tilde{h}_{\tilde{x}} + \tilde{C}_{\tilde{z}}]}{\sqrt{1 + \tilde{h}_{\tilde{x}}^2}} = S_c\tilde{C}. \quad (2.12)$$

Notice that adhesion of nanoparticles to the biofilm surface in equation (2.12) is the dominant mode of nanoparticle capture by the biofilm.

Likewise, a second flux condition is imposed at the fluid/biofilm interface at $\tilde{z} = \tilde{h}(\tilde{x})$:

$$D_B \nabla \tilde{C}_B \cdot \hat{n} = S_c \tilde{C}, \quad (2.13)$$

or

$$\frac{D_B[-\tilde{C}_{B,\tilde{x}}\tilde{h}_{\tilde{x}} + \tilde{C}_{B,\tilde{z}}]}{\sqrt{1 + \tilde{h}_{\tilde{x}}^2}} = S_c \tilde{C}. \quad (2.14)$$

We assume a no slip boundary condition

$$\tilde{u} = \tilde{w} = 0 \quad (2.15)$$

at the top of the flow cell $\tilde{z} = d$ and at the biofilm interface $\tilde{z} = \tilde{h}(\tilde{x})$.

The flux of particles passing through the upper and lower walls of the flow cell satisfy

$$\tilde{C}_{\tilde{z}}(\tilde{x}, d, \tilde{t}) = 0 \quad (2.16)$$

and

$$\tilde{C}_{B,\tilde{z}}(\tilde{x}, 0, \tilde{t}) = 0, \quad (2.17)$$

respectively.

Finally, the volumetric flow rate Q of the carrier fluid is given by

$$Q = 1 \int_{\tilde{h}}^d \tilde{u} d\tilde{z}. \quad (2.18)$$

Here the number 1 cm represents the width of the flow cell, where the third dimension (width of the cell) is suppressed.

Initially at $\tilde{t} = 0$, the concentrations of nanoparticles in the bulk fluid and the biofilm, respectively, are

$$\tilde{C}(\tilde{x}, \tilde{z}, 0) = 0, \quad (2.19)$$

and

$$\tilde{C}_B(\tilde{x}, \tilde{z}, 0) = 0. \quad (2.20)$$

2.3 Nondimensional Forms of the Simplified Governing Equations and Conditions

First, define the variable

$$\epsilon = \frac{d}{L}, \quad (2.21)$$

where $\epsilon \ll 1$. Now we will non-dimensionalize the governing equations with the scaling constants given in Table (2.1). Figure 2.1 depicts the nondimensionalized flow cell with a mucus barrier atop the biofilm structure.

The Péclet number $P_e = \frac{Q}{D}$ is a dimensionless ratio depicting the ratio of the nanoparticle transport by advection in a fluid to the transport by diffusion in the fluid. The Reynolds number $R_e = \frac{U d \mu}{\rho}$ is a dimensionless number describing the ratio of viscous forces to inertial forces within the fluid. From equation (2.9), $\frac{D_B}{D} \ll 1$, so we define

Table 2.1: System variables, characteristic scalings and their units

horizontal coordinate	\tilde{x}	L	cm
vertical coordinate	\tilde{z}	d	cm
biofilm height	\tilde{h}	d	cm
time	\tilde{t}	$\frac{d^2}{D_B}$	s
x -velocity	U	$\frac{Q}{d}$	$\frac{\text{cm}}{\text{s}}$
z -velocity	W	$\epsilon \frac{Q}{d}$	$\frac{\text{cm}}{\text{s}}$
pressure	P^*	$\frac{\mu Q}{\epsilon d^2}$	Pa
biofilm concentration	\tilde{C}_B	A	$\frac{\text{g}}{\text{cm}^2}$
fluid concentration	\tilde{C}	A	$\frac{\text{g}}{\text{cm}^3}$

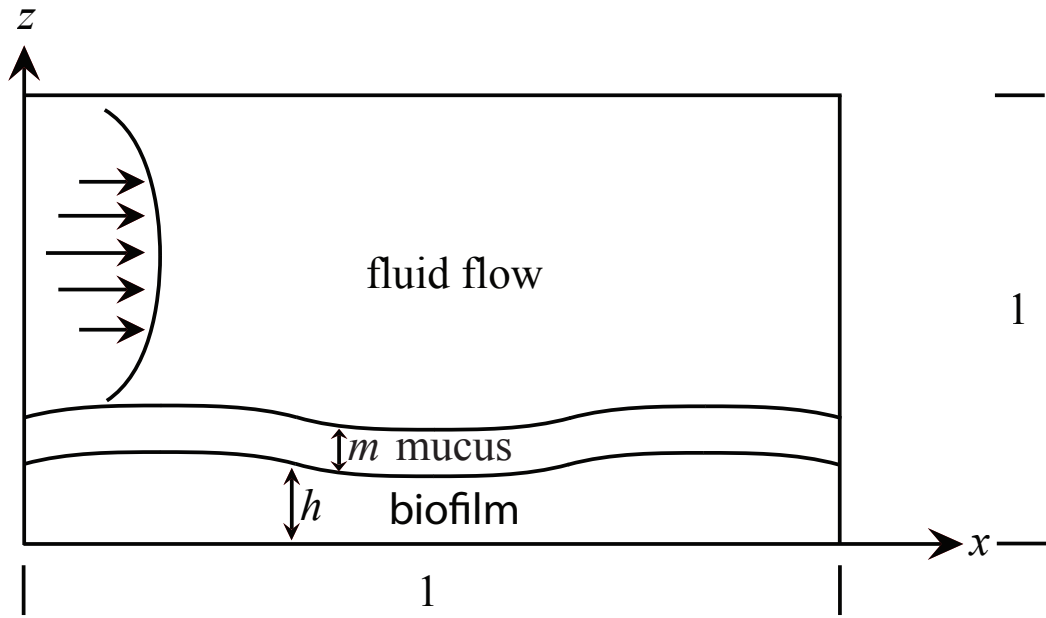


Figure 2.1: The nondimensionalized schematic of the parallel-plate flow cell. In addition to the biofilm on the substrate, a mucus layer approximately 10% the height of the biofilm is added atop the biofilm.

$$\epsilon \hat{D} = \frac{D_B}{D}. \quad (2.22)$$

Hence \hat{D} is an $O(1)$ constant.

These functional groups are used to develop the following non-dimensional governing equations, boundary conditions and initial conditions. The equations of fluid flow are defined in the fluid region where $x \in [0, 1]$ and $z \in [h, 1]$:

$$R_e \epsilon [uu_x + wu_z] = -P_x + \epsilon u_{xx} + u_{zz} \quad (2.23)$$

$$R_e \epsilon [uw_x + ww_z] = -P_z + \epsilon^2 [\epsilon^2 w_{xx} + w_{zz}] \quad (2.24)$$

$$u_x + w_z = 0 \quad (2.25)$$

$$1 = \int_h^1 u dz \quad (2.26)$$

with boundary conditions

$$u(x, h) = u(x, 1) = 0 \quad (2.27)$$

$$w(x, h) = w(x, 1) = 0. \quad (2.28)$$

The equations of nanoparticle concentration in the fluid are defined in the fluid region where $x \in [0, 1]$ and $z \in [h, 1]$:

$$\hat{D} \epsilon C_t + \epsilon P_e [uc_x + wc_z] = \epsilon^2 C_{xx} + C_{zz}, \quad (2.29)$$

$$(2.30)$$

with boundary conditions

$$\frac{-\epsilon^2 C_x h_x + C_z}{\sqrt{1 + \epsilon^2 h_x^2}} = \frac{S_c d}{D} C \quad (2.31)$$

$$C_z(x, 1, t) = 0 \quad (2.32)$$

$$C(0, z, t) = 1 - H(t - t_{inj}). \quad (2.33)$$

and initial condition

$$C(x, z, 0) = 0 \quad (2.34)$$

The equations of nano particle concentration in the biofilm are defined in the region $x \in [0, 1]$ and $z \in [h, 1]$:

$$C_{B,t} = \epsilon^2 C_{B,xx} + C_{B,zz} \quad (2.35)$$

with the boundary conditions

$$C_{B,z}(x, 0, t) = 0. \quad (2.36)$$

$$\frac{-\epsilon^2 C_{B,x} h_x + C_{B,z}}{\sqrt{1 + \epsilon^2 h_x^2}} = \frac{S_c d}{D} C = \frac{S_c d}{D_B} \frac{D_B}{D} C = \frac{S_c d}{D_B} \epsilon \hat{D} C \quad (2.37)$$

and initial condition

$$C_B(x, z, 0) = 0. \quad (2.38)$$

CHAPTER III

SOLUTION PROCEDURE

3.1 Asymptotic Techniques

We make use of the dependence of equations (2.23)-(2.36) on the aspect ratio ϵ in our solution procedure to develop asymptotic equations of the system. We will then solve the leading order solutions numerically. Despite being leading order, a majority of the physics can be obtained from such a method and can be used to test the validity of numerical solutions of the higher order equations.

We begin by assuming all system dependent variables can be expanded asymptotically. With this ansatz, P has the form

$$P = P_0 + \epsilon P_1 + \dots \quad (3.1)$$

Likewise, the other dependent variables of the system have a similar form:

$$u = u_0 + \epsilon u_1 + \dots \quad (3.2)$$

$$w = w_0 + \epsilon w_1 + \dots \quad (3.3)$$

$$C = C_0 + \epsilon C_1 + \dots \quad (3.4)$$

$$C_B = C_{B,0} + \epsilon C_{B,1} + \dots \quad (3.5)$$

Next, we insert the expansions into the system of equations. The $O(1)$ governing equations in the fluid region, where $x \in [0, 1]$ and $z \in [h, 1]$, are those for fluid flow

$$u_{0,x} + w_{0,z} = 0 \quad (3.6)$$

$$P_{0,x} = u_{0,zz} \quad (3.7)$$

$$1 = \int_h^1 u_0 dz. \quad (3.8)$$

$$P_{0,z} = 0. \quad (3.9)$$

and nanoparticle concentration

$$C_{0,zz} = 0, \quad (3.10)$$

which satisfies the boundary conditions

$$C_{0,z}(x, 1, t) = 0 \quad (3.11)$$

$$C_{0,z}(x, h, t) = 0 \quad (3.12)$$

$$C_0(0, z, t) = 1 - H(t - t_0) \quad (3.13)$$

$$(3.14)$$

and the initial condition

$$C_0(x, z, 0) = 0. \quad (3.15)$$

The $O(1)$ equation of nanoparticle concentration in the biofilm region, where $x \in [0, 1]$ and $z \in [0, h]$, is

$$C_{B,0,t} = C_{B,0,zz} \quad (3.16)$$

satisfying the boundary conditions

$$C_{B,0,z}(x, h(x), t) = 0 \quad (3.17)$$

$$C_{B,0,z}(x, 0, t) = 0 \quad (3.18)$$

and the initial condition

$$C_{B,0}(x, z, 0) = 0. \quad (3.19)$$

The input concentration A is not present in the $O(1)$ equations due to nondimensionalization. Therefore, the input concentration is arbitrary, and the solution procedure that follows assumes the input concentration is 1. In the figures of Chapter IV the nanoparticle concentrations represent the fraction of nanoparticles present at a particular grid point with respect to the input concentration. Since the coupled system of equations derived in this chapter are linear, the results of Chapter IV can be scaled to match experiment.

From equations (3.10), (3.11) and (3.12), we see

$$C_0 = C_0(x, t), \quad (3.20)$$

which is independent of the z variable.

To determine $C_0(x, t)$ we only need some of the $O(\epsilon)$ system of equations.

These are

$$\hat{D}C_{0,t} + P_e u_0 C_{0,x} = C_{1,zz}. \quad (3.21)$$

$$C_{1,z}(x, 1, t) = 0 \quad (3.22)$$

$$C_{1,z}(x, h, t) = \frac{S_c d}{D_B} \hat{D}C_0(x, t) \quad (3.23)$$

$$= K \hat{D}C_0(x, t), \quad (3.24)$$

where we define $K = \frac{S_c d}{D_B}$.

Integrating (3.21) with respect to z we find

$$\hat{D}C_{0,t} z + P_e C_{0,x} \int_{h(x)}^z u_0 dz = C_{1,z} + J(x, t), \quad (3.25)$$

where $J(x, t)$ is an arbitrary function. At $z = 1$ and using (3.8), we get

$$\hat{D}C_{0,t} + P_e C_{0,x} = J(x, t), \quad (3.26)$$

and at $z = h$

$$\hat{D}C_{0,t}(x, t)h(x) = C_{1,z}(x, h(x), t) + J(x, t). \quad (3.27)$$

Subtracting equations (3.26) and (3.27) using the interface condition (3.24) we have

$$\hat{D}C_{0,t}[1 - h(x)] + P_e C_{0,x} + K \hat{D}C_0(x, t) = 0. \quad (3.28)$$

In Chapter IV we introduce a mucus layer to the top of the biofilm. From the study by Tang et al. [19], typical mucus thickness in the lungs is on the order of 0.01 cm, and has a mass diffusivity on the order of $D_M = 1.0 \times 10^{-8}$ to $1.0 \times 10^{-12} \frac{\text{cm}^2}{\text{s}}$. Here we have defined the quantity D_M as the mass diffusivity of mucus. When solving equation (3.16) numerically, we decrease the mass diffusivity to be on the order of D_M in the top 10% of the biofilm structure. This will show the effect of mucus on nanoparticle penetration into the biofilm.

3.2 Numerical Solution of the System of Equations

We solve the system of equations given by

$$\hat{D}C_{0,t}[1 - h] + P_e C_{0,x} + K \hat{D}C_0(x, t) = 0 \quad (3.29)$$

with the boundary and initial condition, respectively,

$$C_0(0, t) = 1 - H(t - t_{inj}) \quad (3.30)$$

$$C_0(x, 0) = 0 \quad (3.31)$$

in the fluid region and

$$C_{B,0,t} = C_{B,0,zz} \quad (3.32)$$

in the biofilm satisfying the boundary conditions

$$C_{B,0,z}(x, h(x), t) = KC_0(x, t) \quad (3.33)$$

$$C_{B,0,z}(x, 0, t) = 0 \quad (3.34)$$

and initial condition

$$C_{B,0,z}(x, z, 0) = 0 \quad (3.35)$$

using finite difference methods.

The biofilm concentration equation (3.16) is solved using the Crank-Nicolson method at discrete x locations. Crank-Nicolson is typically used to solve diffusion equations. The method is second order in time, implicit in time, and is unconditionally stable. The discretization of equation (3.16) is

$$\frac{C_{Bk}^{n+1} - C_{Bk}^n}{\Delta t} = \frac{1}{2(\Delta x)^2} \left((C_{Bk-1}^{n+1} - 2C_{Bk}^{n+1} + C_{Bk+1}^{n+1}) + ((C_{Bk-1}^n - 2C_{Bk}^n + C_{Bk+1}^n)) \right), \quad (3.36)$$

where the index n denotes the time t_n for $n = 1, \dots, n_{\max}$ in the domain $t \in [0, 1]$, the index k denotes the vertical position z_k for $k = 1, \dots, k_{\max}$ in the domain $z \in [0, h(x)]$ and the suppressed index i denotes the horizontal position x_i for $i = 1, \dots, i_{\max}$ in the domain $x \in [0, 1]$. Letting $r = \frac{\Delta t}{(\Delta x)^2}$ yields

$$-rC_{Bk-1}^{n+1} + (1 + 2r)C_{Bk}^{n+1} - rC_{Bk+1}^{n+1} = -rC_{Bk-1}^n + (1 - 2r)C_{Bk}^n - rC_{Bk+1}^n. \quad (3.37)$$

This is a tridiagonal problem, so C_B can be solved using a tridiagonal matrix algorithm and the following boundary conditions:

$$C_{B,0}(x, z, 0) = 0 \quad (3.38)$$

$$C_{B,0,z}(x, h(x), t) = KC(x, t) \quad (3.39)$$

$$C_{B,0,z}(x, 0, t) = 0. \quad (3.40)$$

We use the Lax-Wendroff method to solve the flow equation (3.28). The method cannot be applied to the advection-diffusion equation, as it is, because the term $K\hat{D}C_0(x, t)$ can cause numerical instability. In order to put equation (3.28) in the standard form

$$u_t(x, t) + a(x)u_x(x, t) = 0, \quad (3.41)$$

we introduce an integration factor $G(x) = \exp(\frac{K\hat{D}}{P_e}x)$.

Multiplying $G(x)$ through equation (3.28) yields

$$G(x)\hat{D}[1 - h(x)]C_{0,t} + G(x)P_eC_{0,x} + G(x)K\hat{D}C_0(x, t) = \quad (3.42)$$

$$G(x)\hat{D}[1 - h(x)]C_{0,t} + P_e \left[G(x)C_{0,x} + \frac{K\hat{D}}{P_e}G(x)C_0(x, t) \right] = \quad (3.43)$$

$$\left[\hat{D}(1 - h(x))(G(x)C_0(x, t))_t \right] + P_e[G(x)C_0(x, t)]_x = 0. \quad (3.44)$$

Now, let

$$B(x, t) = G(x)C_0(x, t), \quad (3.45)$$

and substituting this into equation (3.44) we find

$$\hat{D}[1 - h(x)]B_t(x, t) + P_e B_x(x, t) = 0. \quad (3.46)$$

We define

$$s(x) = \frac{P_e}{\hat{D}[1 - h(x)]} \quad (3.47)$$

to write equation (3.46) as

$$B_t(x) + s(x)B_x(x) = 0 \quad (3.48)$$

or, equivalently,

$$B_t(x, t) = -s(x)B_x(x, t). \quad (3.49)$$

The standard Lax-Wendroff algorithm must be modified to account for the variable wave speed $s(x)$. The series expansion

$$B_i^{n+1} = (B)_i^n + \Delta t(B_t)_i^{n+1} + \frac{\Delta t^2}{2!}(B_{tt})_i^n \quad (3.50)$$

is expressed by converting the time derivatives to spatial derivatives:

$$B_{tt}(x, t) = (B_t(x))_t \quad (3.51)$$

$$= -s(x)[B_t(x, t)]_x \quad (3.52)$$

$$= -s(x)[-s(x)B_x(x, t)]_x \quad (3.53)$$

$$= s(x)[s'(x)B_x(x, t) + s(x)B_{xx}(x, t)] \quad (3.54)$$

$$= s(x)s'(x)B_x(x, t) + s^2(x)B_{xx}(x, t). \quad (3.55)$$

Substituting equation (3.49) and (3.55) into equation (3.50) we obtain

$$B_i^{n+1} = (B)_i^n + \Delta t [s_i(B_x)_i^n] + \frac{1}{2}\Delta t^2 [s_i(s')_i(B_x)_i^n + (s^2)_i(B_{xx})_i^n]. \quad (3.56)$$

Once $B(x, t)$ is computed, we can solve

$$C_0(x, t) = \frac{B(x, t)}{G(x)} \quad (3.57)$$

to obtain the concentration of nanoparticles in the fluid region.

Finally, the Heaviside function of equation (2.33) denotes the entry condition of the concentration plug. The Lax-Wendroff scheme can produce numerical error when computing finite differences in the sharp corners of the Heaviside function. We therefore smooth the Heaviside using hyperbolic tangents

$$H(t - t_0) \approx \frac{1}{2} \left[\tanh \left[0.003 \left(\frac{d^2}{D_B} t - 1000 \right) \right] - \tanh \left[0.003 \left(\frac{d^2}{D_B} t - 900 \right) \right] \right], \quad (3.58)$$

Table 3.1: Values for system variables used in the solution procedure

Flow Rate	Q	$5.0 \times 10^{-5}, 5.0 \times 10^{-6}$	$\frac{\text{cm}^3}{\text{s}}$
Mass Diffusivity in Fluid	D	1.0×10^{-5}	$\frac{\text{cm}^2}{\text{s}}$
Mass Diffusivity in Biofilm	D_B	$1.0 \times 10^{-7}, 1.0 \times 10^{-8}, 1.0 \times 10^{-9}$	$\frac{\text{cm}^2}{\text{s}}$
Mass Diffusivity in Mucus	D_M	$1.0 \times 10^{-9}, 1.0 \times 10^{-11}$	$\frac{\text{cm}^2}{\text{s}}$
Sticking Coefficient	S_c	$1.0 \times 10^{-4}, 1.0 \times 10^{-5}, 1.0 \times 10^{-6}$	$\frac{\text{cm}}{\text{s}}$
Length of the Flow Cell	L	4.0	cm
Height of the Flow Cell	d	0.1	cm
Input Concentration	A	4.0×10^{-5}	$\frac{\text{g}}{\text{cm}^3}$

where the numbers 1000 and 900 denote the time of ramp up and ramp down, respectively. We introduce a time delay for the boundary condition equation (3.58). This lag in time allows the concentration plug to ramp up smoothly avoiding the numerical oscillations found in Lax-Wendroff solutions at sharp gradients.

Table 3.1 shows the values of the system parameters used in the solution procedure. We do not know the values of mass diffusivity in biofilm D_B , the sticking coefficient of polymer-PLGA nanoparticles S_c , or the average air flow rates in the deep passages of the lungs Q , so we vary these values over several orders of magnitude to illustrate the sensitivity of the results to errors in parameter measurements. Since the system of equations is linear, the input concentration A is kept nondimensionalized in the presentation of the results in Chapter IV.

CHAPTER IV

RESULTS

We now present the numerical results in two parts. In the first section we explore the effects that varying the system parameters of mass diffusivity, flow rate and particle adhesion have on the solution. In the second section a mucus layer is added over the biofilm's surface to simulate an additional physical barrier for particles to penetrate.

4.1 Effects of System Variables on Nanoparticle Concentration

The goal in this section is to show that the numerical method (1) accurately describes the concentration plug flowing through the system, (2) produces reasonable concentration profiles and (3) can predict the effects of varying system parameters.

All cases simulate a particle injection time of 15 minutes over the biofilm surface and an observation period of 24 hours. During that time, concentration data is taken, which we display in the following graphs. The sinusoidal biofilm height $h(x)$ has a baseline nondimensional height of 0.1, amplitude 0.005 and wave number 10. The grid spacings for the simulations are $\Delta x = 1.0 \times 10^{-3}$, $\Delta t = 1.0 \times 10^{-7}$ and $\Delta z(x) = \frac{h(x)}{100}$. The length and width of the flow cell are used nondimensionally in the computation and we then dimensionalize the spatial coordinates for presenting the figures that follow.

Table 4.1: System parameters used for 4.1.1

Flow Rate	Q	5.0×10^{-5}	$\frac{\text{cm}^3}{\text{s}}$
Mass Diffusivity of Biofilm	D_B	$1.0 \times 10^{-7}, 1 \times 10^{-8}, 1.0 \times 10^{-9}$	$\frac{\text{cm}^2}{\text{s}}$
Sticking Coefficient	S_c	1.0×10^{-7}	$\frac{\text{cm}}{\text{s}}$

4.1.1 Effects of Biofilm Mass Diffusivity Properties

In this subsection, we simulate various magnitudes of the mass diffusivity of the biofilm constant D_B that appears in equation (2.8). The mass diffusivity of nanoparticles in the fluid has the value $D = 1.0 \times 10^{-5} \frac{\text{cm}^2}{\text{s}}$ taken from Drury [15, 16]. We vary the mass diffusivity of D_B by factors of 10, and the values used are shown in Table 4.1. The results of these simulations show that the mechanism for diffusing nanoparticles into the biofilm produces realistic results.

For the solutions presented in this subsection, the Péclet number $P_e = 5.0$ and the sticking coefficient $S_c = 1.0 \times 10^{-7} \frac{\text{cm}}{\text{s}}$ ($K = 0.04$) are used. Table 4.1 shows the system variables used for this subsection. The mass diffusivity in the biofilm D_B is unknown, so since we are assuming $D_B \ll D$, we decrease the order of magnitude of D_B by factors of 10.

Figure 4.1 depicts the changes that occur when D_B is decreased from 1.0×10^{-7} to 1.0×10^{-8} and $1.0 \times 10^{-9} \frac{\text{cm}^2}{\text{s}}$. Concentrations C_B are plotted at the horizontal position $x = 1 \text{ cm}$ and at time $t = 1.2 \text{ hours}$. When $D_B = 1.0 \times 10^{-7} \frac{\text{cm}^2}{\text{s}}$, we see an exponential decrease in concentration from the surface of the biofilm to the substrate.

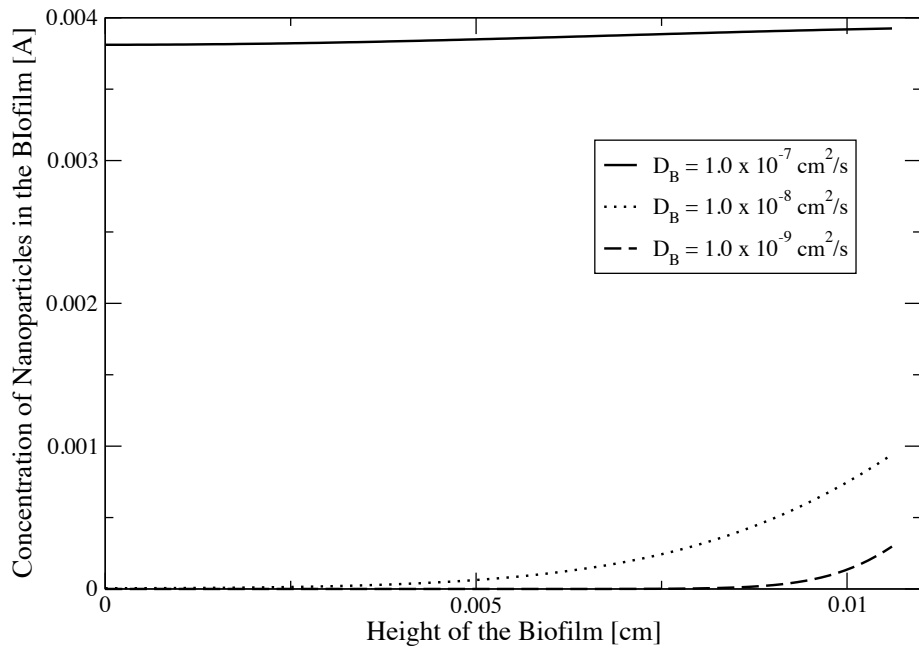


Figure 4.1: This simulation compares the changes mass diffusivity of the biofilm D_B has on the concentration profiles in the biofilm. $D_B = 1.0 \times 10^{-7}$, 1.0×10^{-8} and $1.0 \times 10^{-9} \frac{\text{cm}^2}{\text{s}}$, and the three lines represent concentration values as a function of biofilm depth at the horizontal position $x = 1 \text{ cm}$ and at the time $t = 72 \text{ min}$ in the flow cell.

Even at depth, a noticeable concentration of nanoparticles is present. When the mass diffusivity of biofilm is decreased to 1.0×10^{-8} we see a dramatic decrease in concentration throughout the biofilm and the exponential decay of concentration. Finally, a D_B value of 1.0×10^{-9} prevents nanoparticles from penetrating the depth of the biofilm. As the concentration plug flows past the $x = 1$ cm position, D_B is too small for any significant diffusive penetration into the biofilm.

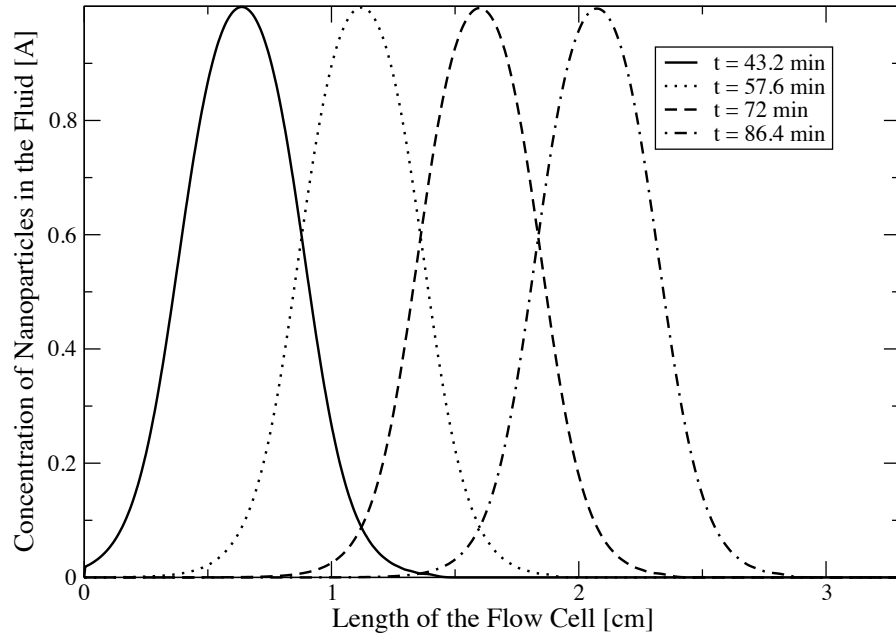


Figure 4.2: The concentration plug flowing through the flow cell is depicted. We show four concentration profiles occurring at times between 43.2 min and 86.4 min. The dilute concentration of the plug and the relatively low sticking coefficient K prevent the profile from changing radically. Also, the profile of the biofilm surface does not influence the spacing between peaks.

Table 4.2: System parameters used for subsection 4.1.2

Flow Rate	Q	$5.0 \times 10^{-5}, 5.0 \times 10^{-6}$	$\frac{\text{cm}^3}{\text{s}}$
Mass Diffusivity of Biofilm	D_B	1.0×10^{-7}	$\frac{\text{cm}^2}{\text{s}}$
Sticking Coefficient	S_c	1.0×10^{-7}	$\frac{\text{cm}}{\text{s}}$

Figure 4.2 shows the concentration profile of the nanoparticle plug passing through the flow cell at four consecutive times. The dilute concentration of the plug and the relatively low sticking coefficient K prevent the profile from changing radically. At first order the morphology of the biofilm's surface does not alter the flow of nanoparticles through the flow cell.

4.1.2 Effects of Flow Rate on Nanoparticle Penetration into Biofilm

In this subsection we vary the flow rate parameter Q , which influences the Péclet number $P_e = \frac{Q}{D}$ and hence the advection speed. We show the influence changing the flow rate Q can have on the profile of the nanoparticle plug and the concentrations in the biofilm.

Table 4.2 gives the values of system parameters used in this subsection. We use $D_B = 1.0 \times 10^{-7} \frac{\text{cm}^2}{\text{s}}$ and a sticking coefficient $S_c = 1.0 \times 10^{-7} \frac{\text{cm}}{\text{s}}$, and we vary Q from 1.0×10^{-5} to $1.0 \times 10^{-6} \frac{\text{cm}^3}{\text{s}}$.

Figure 4.3 depicts the time evolution of nanoparticle concentrations in the biofilm at $x = 1$ cm. From Figure 4.2, the plug begins to pass over the $x = 1$ cm position at time $t = 43.2$ min. At this time nanoparticles begin to diffuse into

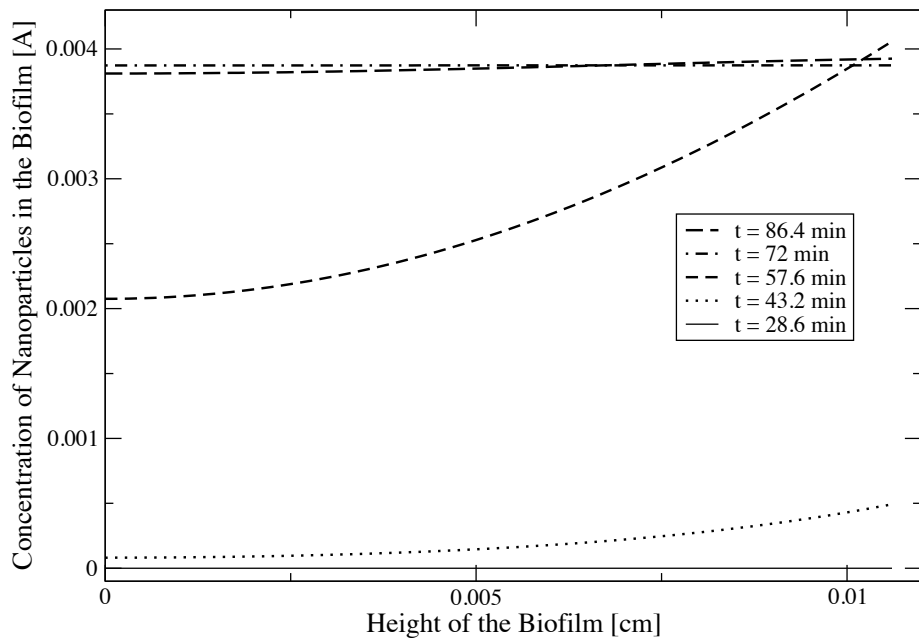


Figure 4.3: The time evolution of concentration of nanoparticles in the biofilm C_B with flow rate $Q = 1.0 \times 10^{-5} \frac{\text{cm}^3}{\text{s}}$. The biofilm concentration function C_B is measured at $x = 1.0 \text{ cm}$, and we show the concentration profile from time $t = 28.6 \text{ min}$ to $t = 86.4 \text{ min}$.

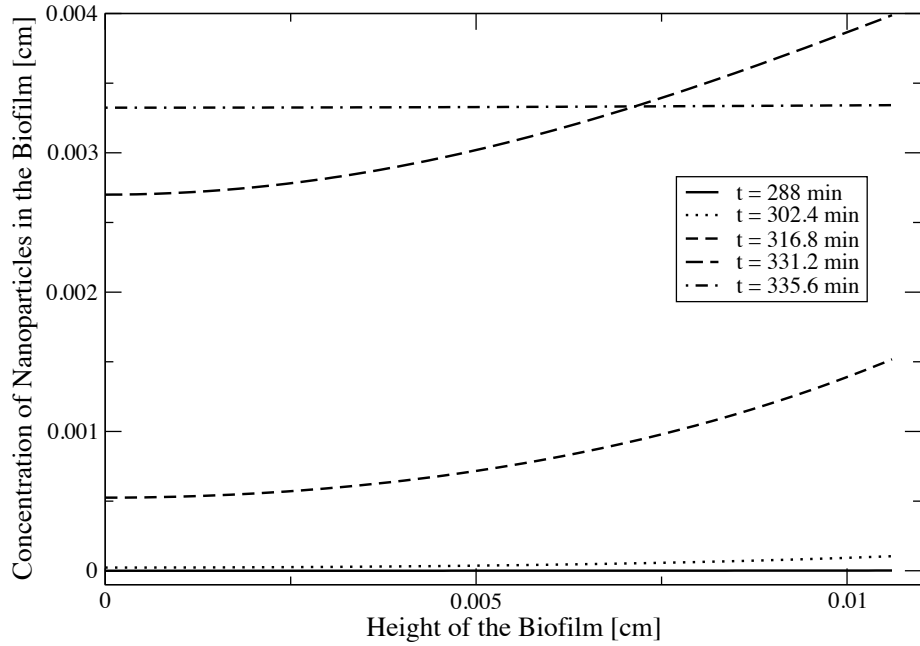


Figure 4.4: The time evolution of nanoparticle concentrations in the biofilm. The flow rate is decreased to $1.0 \times 10^{-6} \frac{\text{cm}^3}{\text{s}}$, and we see the concentration of nanoparticles begins to rise at time $t = 302.4$ min. The time evolution of concentration is like that of Figure 4.3, but due to the smaller flow rate Q , the flux of particles occurs over a greater time period. The concentration profile at $t = 331.2$ min has a more dramatic rise as a result of the decreased flow rate.

the biofilm, which is depicted in Figure 4.3 by a nonzero concentration profile at $t = 43.2$ min. The concentration of nanoparticles increases rapidly as the bulk of the plug passes over the biofilm. After the plug has passed the 1 cm position, the nanoparticles diffuse to a homogenous concentration in the z coordinate.

We decrease the flow rate Q from 1.0×10^{-5} to $1.0 \times 10^{-6} \frac{\text{cm}^3}{\text{s}}$, and results are shown in Figure 4.4 and Figure 4.5. Figure 4.4 shows the time evolution of nanoparticle concentrations in the biofilm, and we see the concentration of nanoparticles begins to rise over 28 minutes before reaching a homogenous concentration of nanoparticles in the vertical direction. Figure 4.5 depicts the narrow concentration profile resulting from the decreased flow rate. By comparing Figures 4.2 and 4.5 we can see the decreased wave speed causes the profile of the plug to narrow and to move more slowly through the flow cell. The concentration profile in Figure 4.4, however, is similar in form to the evolution depicted in Figure 4.3. As a result, such low flow rates have little effect on nanoparticle concentration profiles in the biofilm.

4.1.3 Effects of Sticking Coefficient on Nanoparticle Concentration

In this subsection, we vary the sticking coefficient parameter S_c , which influences the coefficient group $K = \frac{S_{cd}}{D_B}$. We illustrate the effects of the sticking coefficient on concentration profiles in the fluid region and the effects it has on concentrations in the biofilm.

Table 4.3 gives the values of system parameters used in this subsection. We use $D_B = 1.0 \times 10^{-7} \frac{\text{cm}^2}{\text{s}}$ and a flow rate $Q = 1.0 \times 10^{-5} \frac{\text{cm}^3}{\text{s}}$, and we vary S_c using the

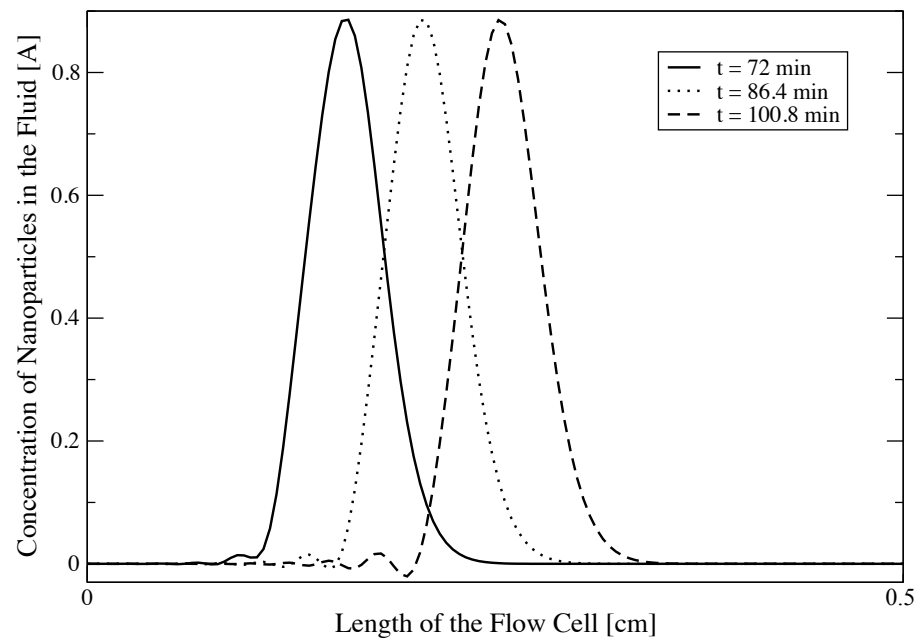


Figure 4.5: This figure shows the narrow concentration profile resulting from decreasing the flow rate Q from 1.0×10^{-5} to $1.0 \times 10^{-6} \frac{\text{cm}^3}{\text{s}}$.

Table 4.3: System parameters used for subsection 4.1.3

Flow Rate	Q	5.0×10^{-5}	$\frac{\text{cm}^3}{\text{s}}$
Mass Diffusivity of Biofilm	D_B	1.0×10^{-7}	$\frac{\text{cm}^2}{\text{s}}$
Sticking Coefficient	S_c	$1.0 \times 10^{-7}, 1.0 \times 10^{-6}, 1.0 \times 10^{-5}$	$\frac{\text{cm}}{\text{s}}$

values 1.0×10^{-8} , 1.0×10^{-7} , and $1.0 \times 10^{-6} \frac{\text{cm}}{\text{s}}$. We will show the sticking coefficient parameter has the greatest effect on concentration profiles.

Figure 4.6 shows the concentration profile for the case $Q = 1.0 \times 10^{-5}$, $D_B = 1.0 \times 10^{-7} \frac{\text{cm}^3}{\text{s}}$ and sticking coefficient $S_c = 1.0 \times 10^{-7} \frac{\text{cm}}{\text{s}}$ in the biofilm. We see little evidence of diffusion or spreading of the curve. In Figure 4.7 we show the concentration profile of the nanoparticle plug passing through the flow cell with an increase in the sticking coefficient S_c . By changing the sticking coefficient from 1.0×10^{-7} to $1.0 \times 10^{-6} \frac{\text{cm}}{\text{s}}$ we see an increased absorption of nanoparticles into the biofilm, which causes a decrease in the concentration profile amplitude as shown in Figure 4.7.

Figure 4.8 depicts an increased sticking coefficient S_c . We use $S_c = 1.0 \times 10^{-5} \frac{\text{cm}}{\text{s}}$ which causes spreading of the concentration profile. The amplitude of the concentration profile may decrease due to rapid nanoparticle adhesion thereby decreasing the concentration level in the plug.

Figure ?? shows the surface plots of nanoparticle concentration in the biofilm for the three values of the sticking coefficient S_c . The three surfaces are similar in form

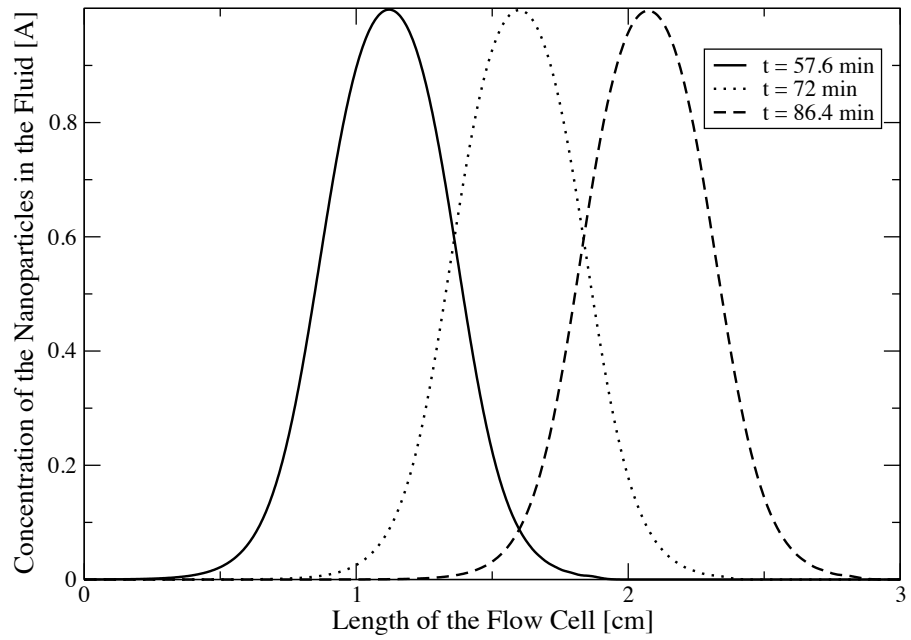


Figure 4.6: The concentration profile for the case $Q = 1.0 \times 10^{-5} \frac{\text{cm}^3}{\text{s}}$, $D_B = 1.0 \times 10^{-7} \frac{\text{cm}^2}{\text{s}}$ and $S_c = 1.0 \times 10^{-7} \frac{\text{cm}}{\text{s}}$.

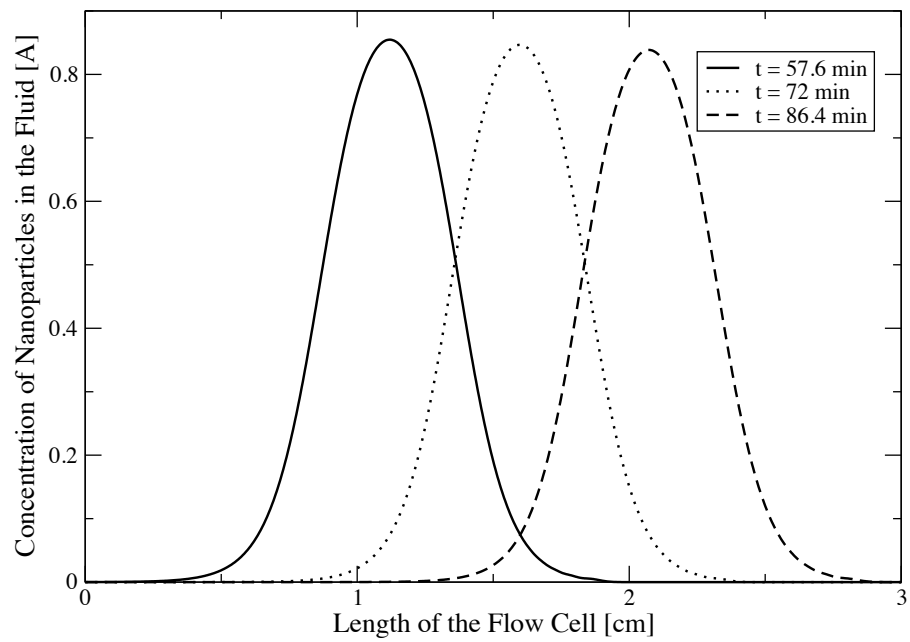


Figure 4.7: The concentration profile of the nanoparticle plug passing through the flow cell with an increase in the sticking coefficient S_c . By changing the sticking coefficient from 1.0×10^{-7} to $1.0 \times 10^{-6} \frac{\text{cm}}{\text{s}}$, we can begin to see absorption of nanoparticles into the biofilm as time progresses from $t = 57.6$ to $t = 86.4$ min.

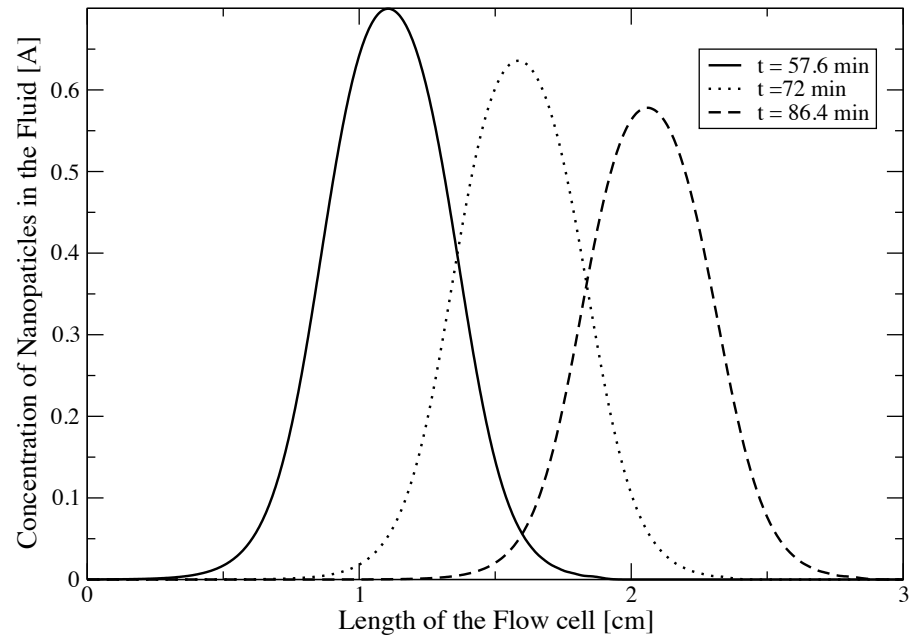


Figure 4.8: The concentration profile for the case $Q = 1.0 \times 10^{-5} \frac{\text{cm}^3}{\text{s}}$, $D_B = 1.0 \times 10^{-7} \frac{\text{cm}^2}{\text{s}}$ and $S_c = 1.0 \times 10^{-5} \frac{\text{cm}}{\text{s}}$.

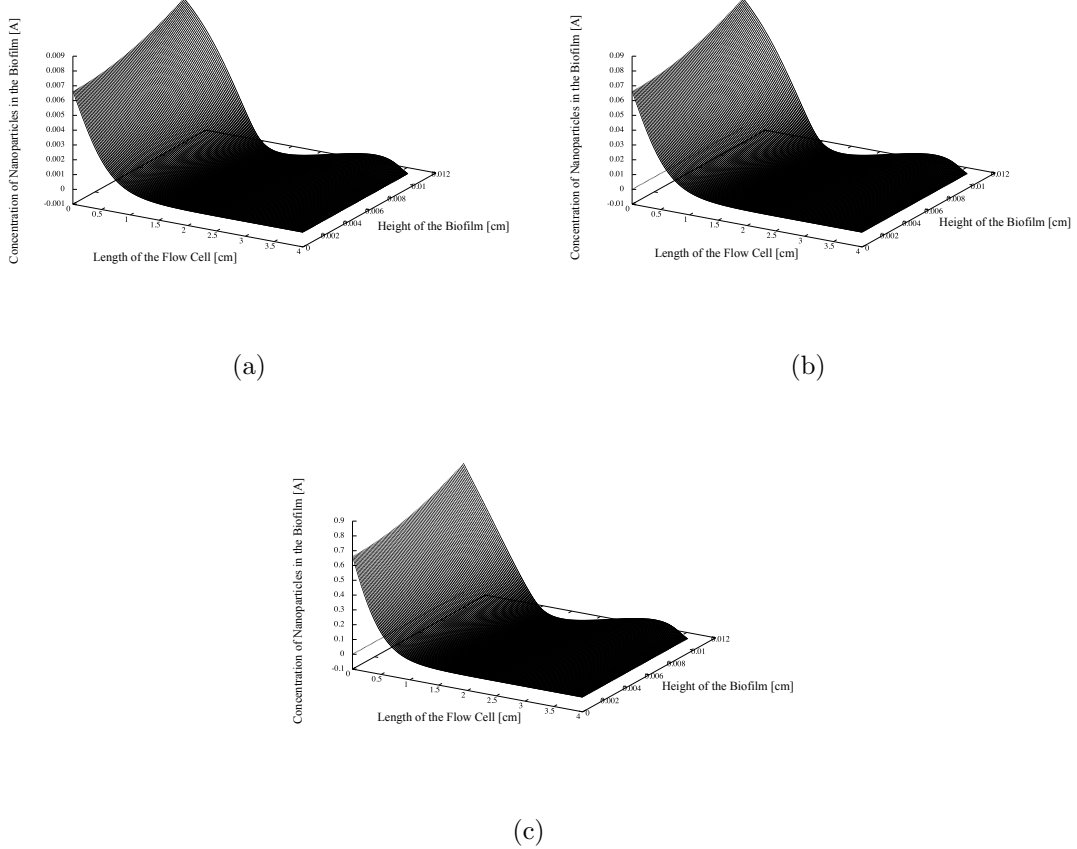


Figure 4.9: Surface plots for three values of the sticking coefficient (a) $S_c = 1.0 \times 10^{-7}$, (b) 1.0×10^{-6} , (c) $1.0 \times 10^{-5} \frac{\text{cm}}{\text{s}}$.

and differ in magnitude. The flux of nanoparticles passing through the fluid/biofilm interface is proportional to the sticking coefficient S_c as shown in equation (3.24), so as expected, increasing the sticking coefficient increases the flux of particles entering the biofilm's surface.

4.2 Effects of a Mucus Barrier on Nanoparticle Absorption

Our goal in this section is to show (1) how mucus barriers affect particle penetration into the depths of the biofilm and (2) how the model is able to adapt to varying surface morphologies at the interface.

As in the previous section all cases simulate a particle injection time of 15 minutes over the biofilm surface and an observation period of 24 hours. Again, the sinusoidal biofilm height $h(x)$ has an initial nondimensional baseline of 0.1 and a wave number of 100. The curve's amplitude is increased to 0.08 creating large variations in the sinusoidal surface. The grid spacings for the simulations remain the same at $\Delta x = 1.0 \times 10^{-3}$ cm, $\Delta t = 1.0 \times 10^{-7}$ s and $\Delta z(x) = \frac{h(x)}{100}$ cm.

Unlike previous simulations, a layer of mucus is introduced to the top of the biofilm structure. This additional barrier is assumed to conform to the surface morphology of the biofilm.

4.2.1 Effects of Mucus Barriers on Nanoparticle Concentrations in the Biofilm

For this subsection, we vary the mass diffusivity of mucus D_M . We illustrate the effect varying the mass diffusivity of the mucus D_M has on nanoparticle concentration profiles in the fluid region, mucus, and biofilm regions. The system parameters used in the following graphs are depicted in Table 4.4.

Figure 4.10 shows the introduction of a mucus to the top 10% of the biofilm structure. The mass diffusivity of mucus $D_M = 1.0 \times 10^{-8} \frac{\text{cm}^2}{\text{s}}$ dramatically decreases concentration percentages in both the mucus and the biofilm. We see in the mucus

Table 4.4: System parameters used for 4.2.1

Flow Rate	Q	5.0×10^{-8}	$\frac{\text{cm}^3}{\text{s}}$
Mass Diffusivity of Biofilm	D_B	1.0×10^{-7}	$\frac{\text{cm}^2}{\text{s}}$
Sticking Coefficient	S_c	1.0×10^{-7}	$\frac{\text{cm}}{\text{s}}$
Mass Diffusivity of Mucus	D_M	$1.0 \times 10^{-6}, 1.0 \times 10^{-8}, 1.0 \times 10^{-9}$	$\frac{\text{cm}^2}{\text{s}}$

region a rapid exponential decrease in nanoparticle concentration followed by much lower concentration levels in the biofilm. This effect is more evident in the next scenario when the mass diffusivity of the mucus barrier D_M is decreased by another order of magnitude.

Figure 4.11 depicts the result of decreasing the mass diffusivity in the mucus D_M to $1.0 \times 10^{-9} \frac{\text{cm}^2}{\text{s}}$, and the graph shows an even greater decrease in nanoparticle concentration levels in both the mucus and the biofilm. We see the decreased mass diffusivity of mucus D_M causes a more rapid exponential decay in the mucus region, and even lower concentrations of nanoparticles in the biofilm. This illustrates the complications that arise from delivering nanoparticles to infections in deep lung passages. Mucus is an effective barrier preventing nanoparticles from reaching effective concentration levels in the biofilm to prohibit bacterial growth.

A dense surface coating of poly(ethylene glycol) (PEG) can allow coated nanoparticles to pass through mucus barriers with an increased mass diffusivity in mucus D_M when compared to uncoated nanoparticles. The series of papers by Hanes

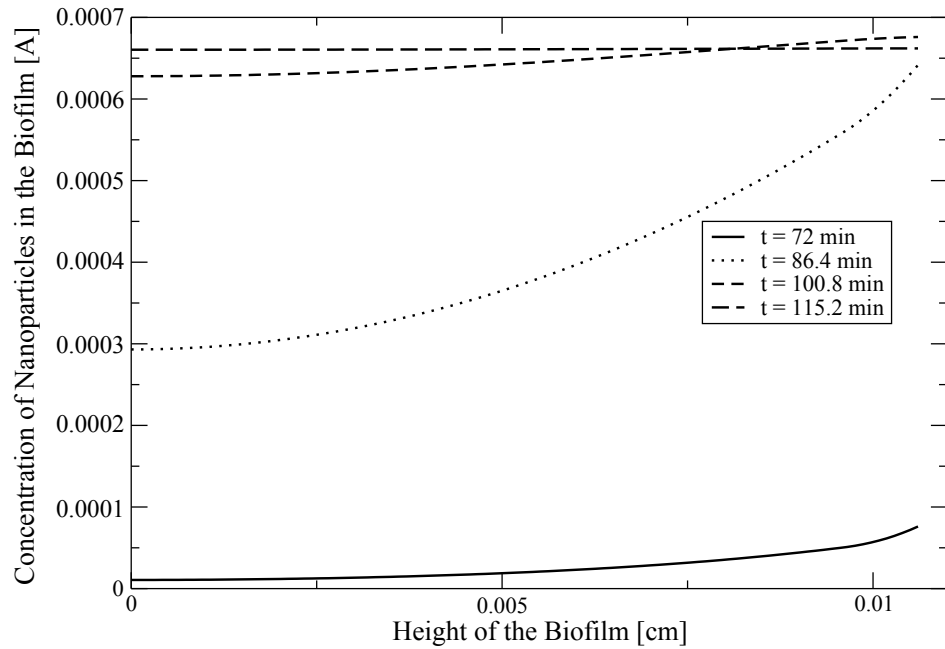


Figure 4.10: The introduction of mucus to the top 10% of the biofilm structure is depicted in this figure. The mass diffusivity of mucus $D_M = 1.0 \times 10^{-8} \frac{\text{cm}^2}{\text{s}}$ rapidly decreases concentration profiles with magnitudes much less than those found in a pure biofilm substrate. We see a region of exponential decrease at an increased rate in the top tenth of the biofilm followed by a much gentler decrease in concentration of nanoparticles at depths in the biofilm.

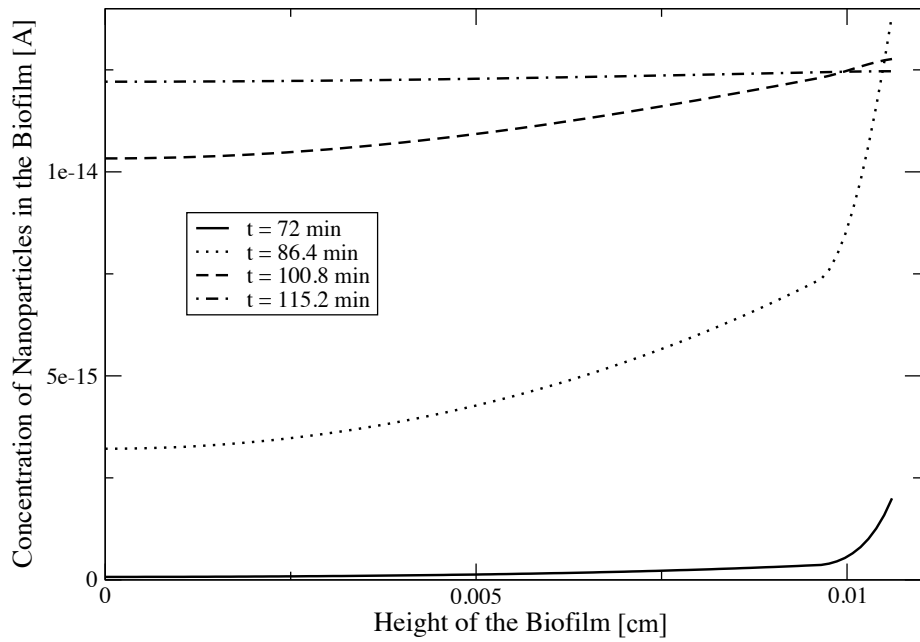


Figure 4.11: This figure depicts the effects of a decreased mucus mass diffusivity constant $D_M = 1.0 \times 10^{-9} \frac{\text{cm}^2}{\text{s}}$ on the nanoparticles' ability to penetrate through the additional mucus barrier. We see a rapid decrease in the concentration profile in the top 10% of the biofilm followed by a shallow exponential decay of concentration into the remaining depth of the biofilm structure.

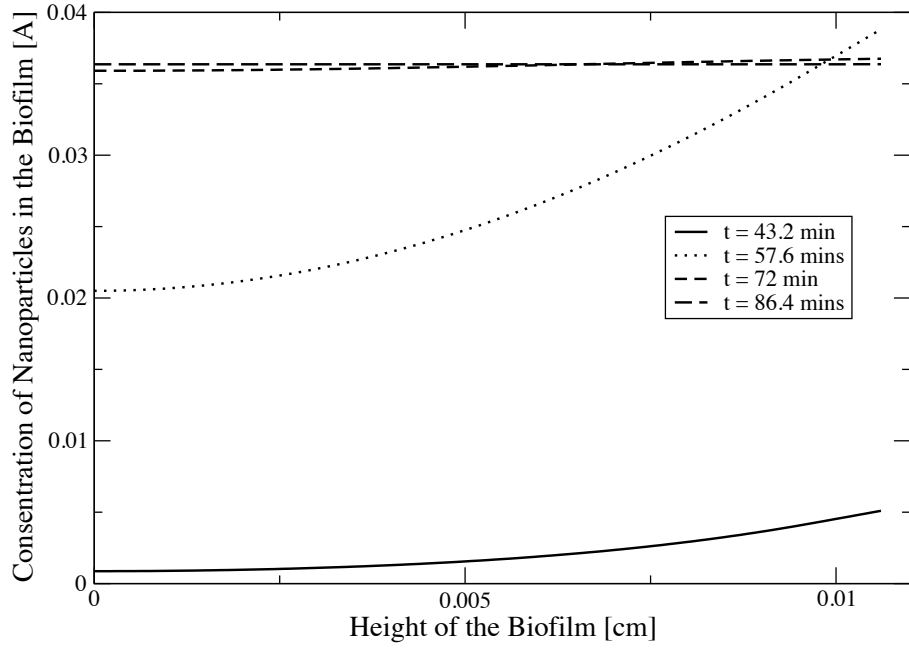


Figure 4.12: The concentratino profile for the case $Q = 1.0 \times 10^{-5} \frac{\text{cm}^3}{\text{s}}$, $D_B = 1.0 \times 10^{-7} \frac{\text{cm}^2}{\text{s}}$, $D_M = 1.0 \times 10^{-6} \frac{\text{cm}^2}{\text{s}}$ and $S_c = 1.0 \times 10^{-7} \frac{\text{cm}}{\text{s}}$.

et al. suggest the mass diffusivity of coated nanoparticles in mucus is orders of magnitude greater than that of uncoated nanoparticles and less than that of nanoparticles diffusing through water. Figure 4.12 depicts the result of increasing the mass diffusivity in the mucus D_M to $1.0 \times 10^{-6} \frac{\text{cm}^2}{\text{s}}$, and the graph shows an increase in nanoparticle concentration in the biofilm compared with that of Figure 4.10.

4.2.2 Effects of a Highly Variable Biofilm Surface Morphology on Nanoparticle Concentrations in the Biofilm with a Mucus Barrier

In this subsection, we introduce the mucus barrier halfway through the flow cell. This is to simulate a partially covered biofilm in the lungs. We vary the amplitude of the biofilm surface greatly. This simulation tests the ability of the method to handle large changes in surface morphology. Biofilms can develop amorphous structures on their surface; therefore, a model describing biofilm structure must be stable for a wide range of surface profiles.

Figure 4.13 shows the flexibility of the model derived in this thesis. The surface morphology of the biofilm and biofilm/mucus interface, which the plug passes over, does not significantly affect the concentration profile in the flow cell. The surface morphology of the biofilm or mucus interface does not have a significant effect on flow or concentration profiles in the fluid and biofilm region respectively.

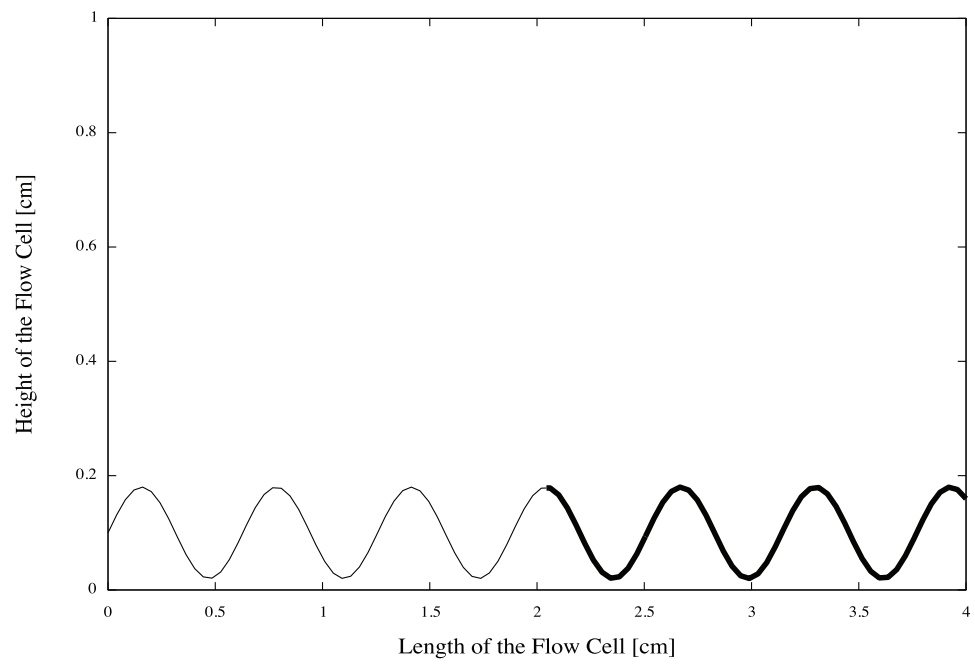
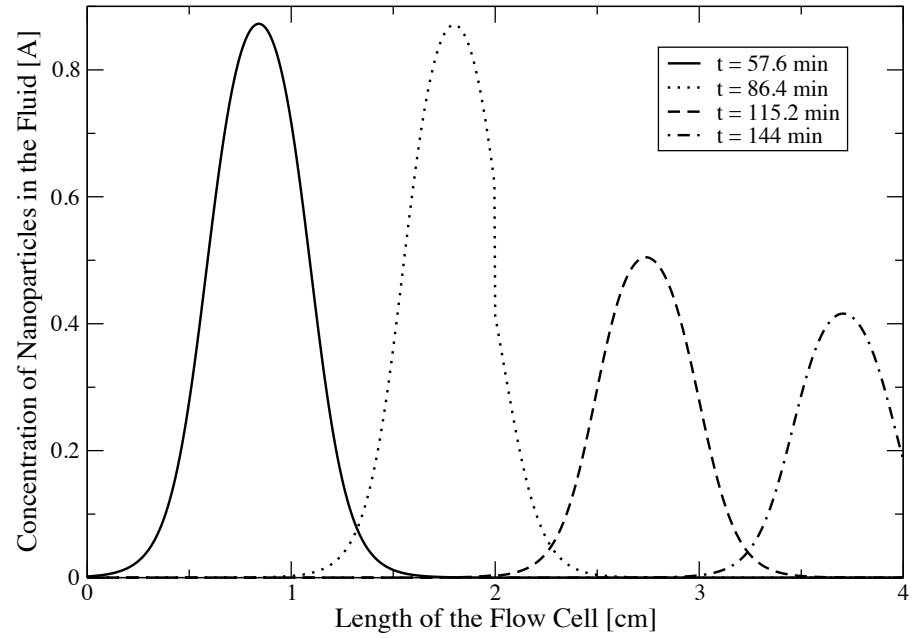


Figure 4.13: This figure shows the flexibility of the method derived in this thesis. The highly variable surface morphology of the biofilm and biofilm/mucus interface, which the plug passes over, do significantly affect the concentration profile in the flow cell.

CHAPTER V

SUMMARY

We derive a two dimensional model of nanoparticle transport in a flow cell, adhesion to a biofilm's surface and the subsequent transport into a planar biofilm. The governing equations were simplified by the following assumptions to produce a system of coupled equations which we solved numerically:

1. The carrier fluid is a well mixed dilute concentration of nanoparticles
2. Fluid flow is parabolic, laminar, and steady state
3. No flux and no slip boundary conditions are imposed at geometry boundaries
4. Nanoparticle adhesion is the main mode of capture at a biofilm surface
5. Diffusion is the dominant form of particle transport in the biofilm
6. System variables can be approximated by asymptotic series.

The nanoparticles are assumed to remain in the biofilm after capture, and we show they quickly diffuse to a uniform concentration after the flow plug has passed.

System parameters such as mass diffusivity of the biofilm, sticking coefficients of the nanoparticles, and flow rate of the carrier fluid through the flow cell are varied. Decreasing the mass diffusivity of the biofilm resulted in a large decrease in

nanoparticle concentration throughout the biofilm's depth. After the concentration plug has passed through the flow cell, the nanoparticles diffuse to a uniform concentration with respect to the z coordinate. The flow rate Q alters the profile of the concentration plug traveling through the flow cell, but large changes in nanoparticle concentrations in the biofilm are not observed as a result of a decreased flow rate. The sticking coefficient S_c parameter limits the flux of nanoparticles passing through the fluid/biofilm interface. As the sticking coefficient is increased, a large increase in nanoparticle concentrations in the biofilm is observed.

A mucus barrier diminishes the ability of polymeric nanoparticles to penetrate deeply into the depth of a biofilm. This research indicates nanoparticles coated with PEG can slip through mucus barriers. The resulting nanoparticle concentration in the biofilm is of the same magnitude as simulations without the additional mucus barrier.

With the model developed in this thesis we need further research to obtain the appropriate values for the system parameters and physical characteristics of polymeric nanoparticles. The information from these studies could improve our model to better resemble nanoparticle deposition in the deep passages of the lung.

BIBLIOGRAPHY

- [1] K. Jackson, R. Keyser, and D. Wozniak. The role of biofilms in airway disease. *Semin Respir Crit Care Med*, 24(6):663–670, 2003.
- [2] G. Zacarias, C. Ferreira, and J. Velasco-Hernandez. Porosity and tortuosity relations as revealed by a mathematical model of biofilm structure. *Journal of Theoretical Biology*, 233:245–251, 2005.
- [3] J. Costerton, S. Stewart, and E. Greenberg. Bacterial biofilms: A common cause of persistent infections. *Science*, 284(5418):1318–1322, 1999.
- [4] P. Stewart and J. Costerton. Antibiotic resistance of bacteria in biofilms. *Lancet*, 358:135–138, 2001.
- [5] N. Sufya, D. Allsion, and P. Gilbert. Clonal variation in maximum specific growth rate and susceptibility towards antimicrobials. *J Appl Microbiol*, 95:1261–1267, 2003.
- [6] N. Cogan and J. Keener. The role of the biofilm matrix in structural development. *Mathematical Medicine and Biology*, 21:147–166, 2004.
- [7] B. Szomolay, I. Klapper, J. Dockery, and P. Stewart. Adaptive responses to antimicrobial agents in biofilms. *Environmental Microbiology*, 7(8):1186–1191, 2005.
- [8] B. Ramsey. Management of pulmonary disease in patients with cystic fibrosis (vol 335, pg 179, 1996). *New England Journal of Medicine*, 335(15):1167–1167, 1996.
- [9] S. Yoon, R. Hennigan, G. Hilliard, U. Ochsner, K. Parvatiyar, M. Kamani, H. Allen, T. DeKievit, P. Gardner, U. Schwab, J. Rowe, B. Iglewski, T. McDermott, R. Mason, D. Wozniak, R. Hancock, M. Parsek, T. Noah, R. Boucher, and D. Hassett. *Pseudomonas aeruginosa* anaerobic respiration in biofilms: Relationships to cystic fibrosis pathogenesis. *Developmental Cell*, 3(4):593 – 603, 2002.

- [10] R. Gibson, J. Burns, and B. Ramsey. Pathophysiology and management of respiratory infections in cystic fibrosis. *Am J Respir Crit Care Med*, 168(8):918–951, 2003.
- [11] A. Lambiase, V. Raia, M. Pezzo, A. Sepe, V. Carnovale, and F. Rossano. Microbiology of airway disease in a cohort of patients with cystic fibrosis. *BMC Infectious Diseases*, 6(1):4–, 2006.
- [12] B. Neumann, H. Bean, J. Beckett, and J. Carless. The flow properties of powders. *Adv Pharm Sci*, 2:191–221, 1967.
- [13] P. Longest and M. Oldham. Numerical and experimental deposition of fine respiratory aerosols: Development of a two-phase drift flux model with near-wall velocity corrections. *Journal of Aerosol Science*, 39(1):48–70, January 2008.
- [14] J. Xi and P. Longest. Transport and deposition of micro-aerosols in realistic and simplified models of the oral airway. *Annals of Biomedical Engineering*, 35:560–581, 2007. 10.1007/s10439-006-9245-y.
- [15] W. Drury, P. Stewart, and W. Characklis. Transport of 1 micrometer latex particles in pseudomonas aeruginosa biofilms. *Biotechnology and Bioengineering*, 42(1):111–117, 1993.
- [16] W. Drury, W. Characklis, and P. Stewart. Interactions of 1 micrometer latex particles in pseudomonas aeruginosa biofilms. *Biotechnology and Bioengineering*, 42(1):1119–1126, June 1993.
- [17] P. Bishop. Biofilm structure and kinetics. *Water Science and Technology*, 36(1):287–294, 1997.
- [18] I. Klapper, C. Rupp, R. Cargo, B. Purvedorj, and P. Stoodley. Viscoelastic fluid description of bacterial biofilm material properties. *Biotechnology and Bioengineering*, 80(3):289–296, 2002.
- [19] B. Tang, M. Dawson, S. Lai, Y. Wang, J. Suk, M. Yang, P. Zeitlin, M. Boyle, J. Fu, and J. Hanes. Biodegradable polymer nanoparticles that rapidly penetrate the human mucus barrier. *Proceedings of the National Academy of Sciences*, 106(46):19268–19273, 2009.
- [20] J. Suh, K. Choy, S. Lai, J. Suk, B. Tang, S. Prabhu, and J. Hanes. Pegylation of nanoparticles improves their cytoplasmic transport. *International Journal of Nanomedicine*, 2(4):735–741, 2007.

- [21] J. Suk, S. Lai, Y. Wang, L. Ensign, P. Zeitlin, M. Boyle, and J. Hanes. The penetration of fresh undiluted sputum expectorated by cystic fibrosis patients by non-adhesive polymer nanoparticles. *Biomaterials*, 30(13):2591 – 2597, 2009.
- [22] Y. Wang, S. Lai, J. Suk, A. Pace, R. Cone, and J. Hanes. Addressing the peg mucoadhesivity paradox to engineer nanoparticles that “slip” through the human mucus barrier. *Angewandte Chemie International Edition*, 47(50):9726–9729, 2008.
- [23] E. Luna, G. Dominguez-Zacarias, C. Ferreira, and J. Velasco-Hernandez. Detachment and diffusive-convective transport in an evolving heterogeneous two-dimensional biofilm hybrid model. *Phys. Rev. E*, 70(6):061909, Dec 2004.

APPENDIX

NUMERICAL SOLVER

C Neubig

C Solves C_t + a*C_x = -K*C, CB_t = CB_zz

program lung5

implicit none

integer i,imax,k,kmax,n,nmax

double precision C(1001,0:1),CB(1001,101,0:1),BB(1001,0:1)

double precision ss(1001),G(1001),sp(1001),dz(1001)

double precision x(1001),z(1001,101),t(100001),RHS(101)

double precision BH(1001),CBz(1001),AL(1001),AM(1001),AR(1001)

double precision output(101),D(101),Bx,Bxx,dx,dt,rx,rz,gpx,gpz

double precision Heaviside,iface,m,m1,mid,p1

double precision Q,DF,DB,Sc,h,L,epsilon,Pe,Dhat,Ka

```
imax = 1001
```

```
kmax = 101
```

```
nmax = 100001
```

```
dx = 1.d-3
```

```
dt = 1.d-5
```

```
m = 1.d-2
```

```
Q = 5.d-8
```

```
DF = 1.d-5
```

```
DB = 1.d-7
```

```
Sc = 1.d-5
```

```
h = .1d0
```

```
L = 4.d0
```

```
epsilon = h/L
```

```
Pe = Q/h/DB
```

```
Dhat = DB/DF/epsilon
```

```
Ka = Sc*h/DB
```

```
C Build x and time grids
```

```
do i=1,imax
```

```

x(i) = 0.d0 + dfloat(i-1)*dx

end do

do n=1,nmax

t(n) = 0.d0 + dfloat(n-1)*dt

end do

do i=1,imax

BH(i) = iface(x(i))

ss(i) = Pe/Dhat/(1.d0-BH(i))

G(i) = exp(ka*x(i)/Pe)

dz(i) = BH(i)/1.d2

do k=1,kmax

z(i,k) = 0.d0 + dfloat(k-1)*dz(i)

end do

end do

do i=2,imax-1

sp(i) = (ss(i+1)-ss(i-1))/(2.d0*dx)

end do

do k=1,kmax

if (k.ge.91) then

D(k) = 1.d-2

```

```
else  
D(k) = 1.d0  
end if  
end do
```

```
C      Initial Conditions
```

```
n = 0  
call ooutfn('lng',chan3(n),cflag,1)  
do i=1,imax  
C(i,0) = 0.d0  
BB(i,0) = C(i,0)*G(i)  
write(1,*) x(i),C(i,0)
```

```
do k=1,kmax  
CB(i,k,0) = 0.d0  
end do  
end do  
close(1)
```

```
C Main Loop
```

```
do n=1,nmax-1
```

C Lax-Wendroff

```
BB(1,1) = Heaviside(t(n+1))*G(1)

do i=2,imax-1

Bx = (BB(i+1,0)-BB(i-1,0))/(2.d0*dx)

Bxx = (BB(i-1,0)-2.d0*BB(i,0)+BB(i+1,0))/dx**2

BB(i,1) = BB(i,0) - dt*ss(i)*Bx

.           + .5d0*dt**2*( ss(i)*sp(i)*Bx+ss(i)**2*Bxx )

C(i,1) = BB(i,1)/G(i)

end do

BB(imax,1) = 2.d0*BB(imax-1,1) - BB(imax-2,1)

C(imax,1) = BB(imax,1)/G(imax)
```

C Crank-Nicolson

```
do i=1,imax

rz = dt/dz(i)**2

AL(1) = 0.d0

AM(1) = 1.d0 + rz

AR(1) = -rz

do k=2,91

AL(k) = -.5d0*rz

AM(k) = 1.d0 + rz

AR(k) = -.5d0*rz
```

```

end do

do k=92,kmax-1

AL(k) = -m*.5d0*rz

AM(k) = 1.d0 + m*rz

AR(k) = -m*.5d0*rz

end do

AL(kmax) = -rz*m

AM(kmax) = 1.d0 + rz*m

AR(kmax) = 0.d0

RHS(1) = (1.d0-rz)*CB(i,1,0) + rz*CB(i,2,0)

do k=2,91

m1 = .5d0*rz*CB(i,k-1,0)

mid = (1.d0-rz)*CB(i,k,0)

p1 = .5d0*rz*CB(i,k+1,0)

RHS(k) = m1 + mid + p1

end do

do k=92,kmax-1

m1 = .5d0*m*rz*CB(i,k-1,0)

mid = (1.d0-rz*m)*CB(i,k,0)

p1 = .5d0*m*rz*CB(i,k+1,0)

RHS(k) = m1 + mid + p1

end do

```

```

RHS(kmax) = (1.d0-rz*m)*CB(i,kmax,0) + rz*m*CB(i,kmax-1,0)
.
. + m*rz*dz(i)*Ka*( C(i,1)+C(i,0) )

call tridiag(AL,AM,AR,RHS,output,kmax)

do k=1,kmax
  CB(i,k,1) = output(k)
end do
end do

stop

end program

```

```

SUBROUTINE tridiag(a,b,c,r,u,n)

implicit none

! Dummy Variables
INTEGER n
double precision a(n),b(n),c(n),r(n),u(n)

! Local Variables
INTEGER j

```

```

double precision bet,gam(n)

!      a is AL, b is AM, c is AR
!      r is rhs, u is output, n is dimension

if(b(1).eq.0.)pause 'tridag: rewrite equations'
bet=b(1)
u(1)=r(1)/bet
do 11 j=2,n
gam(j)=c(j-1)/bet
bet=b(j)-a(j)*gam(j)
if(bet.eq.0.)pause 'tridag failed'
u(j)=(r(j)-a(j)*u(j-1))/bet
11      continue
do 12 j=n-1,1,-1
u(j)=u(j)-gam(j+1)*u(j+1)
12      continue
return
END

C  (C) Copr. 1986-92 Numerical Recipes Software +%6V+j)D2.

```

```
function Heaviside(t)
```

```

implicit none

double precision Heaviside,t

double precision a,T1,T2

c      dimensional: starts at T1=10, ends at T2=T1+900 seconds

T1 = .04d0

T2 = T1 + 900.d0/3600.d0/24.d0

a = 100.d0

Heaviside = .5d0*(tanh(a*(t - T1)) + tanh(a*(T2-t)))

return

end

function iface(x)

implicit none

double precision iface,x

iface = .1d0 + 1.d-2*sin(10.d0*x)

return

end

```